# Studies on a Detection System for Spectator Protons at ANKE

**Inti Lehmann**

**February 2000**

**Institut für Kernphysik**
**Forschungszentrum Jülich**

Universität zu Köln

# Studies on a Detection System for Spectator Protons at ANKE

Aufbau eines Detektions-Systems zum
Spectator-Nachweis an ANKE

Diplomarbeit
von
Inti Lehmann

Februar 2000

Institut für Kernphysik
Forschungszentrum Jülich

# Abstract

One of the physics goals of the ANKE-spectrometer with the proton-beam of the Cooler Synchrotron COSY-Jülich is to study elementary reactions on an effective neutron-target. By identifying the low energetic spectator-protons from the deuterium cluster target, the reactions on the neutron can be tagged.

Silicon-strip detectors in a telescope-like structure of several layers provide the $\Delta$E/E-identification of protons and deuterons over a large dynamic range, as well as track information for these particles.

Results of the measurements at the Cologne Tandem-Accelerator with a well defined proton beam and of a first beam-time at ANKE are presented. The identification of elastically scattered protons and deuterons is used for the absolute luminosity determination. Furthermore it is shown, how the spectator-proton identification will be performed at ANKE in the near future.

# Zusammenfassung

Das Studium der Meson-Produktion, und dabei speziell der $\omega$-Produktion, an einem effektiven Neutronen-Target ist eines der erklärten Ziele der ANKE-Kollaboration am Synchrotron COSY im Forschungszentrum Jülich. Das im September 1999 installierte Deuterium-Cluster-Jet-Target läßt sich durch den Nachweis des von der Reaktion nicht betroffenen sogenannten “Spectator”-Protons als effektives Neutronen-Target verwenden.

Zum Nachweis dieser Spectator-Protonen wurden im Rahmen dieser Diplomarbeit drei Silizium-Detektoren in einer Teleskopstruktur im COSY-Vakuum aufgebaut. Die zwei kritischen Detektoren – ein nur $18\,\mu$m dicker Sperrschichtzähler und ein 5 mm dicker Streifenzähler – wurden auf ihre Tauglichkeit für die Spectator-Messung in einer Strahlzeit am Tandem-Beschleuniger der Universität zu Köln untersucht. Dabei wurden Protonen im Energiebereich von 2 bis 18 MeV benutzt, um die Genauigkeit der Energiemessung, die Ortsauflösung, die Beschränkung der möglichen Winkelauflösung durch Vielfachstreuung und die Durchführbarkeit der Teilchenidentifikation mit einer Kombination aus diesen Detektoren zu studieren.

Bei der ersten Strahlzeit im September 1999 an ANKE mit 2 GeV Protonen-Energie konnten wir mit unserem Aufbau die Luminosität mit Hilfe der elastischen Streuung von Protonen an Deuteronen bestimmen. Es konnte schon jetzt gezeigt werden, daß die Teilchenidentifikation und die Bestimmung ihrer Energie und Winkel tatsächlich in einem Proton-Energiebereich von mindestens 8 bis 30 MeV in der für die $\omega$-Produktion geforderten Auflösung möglich ist.

Die Vorwärtsdetektoren zur Identifikation der bei der $\omega$-Produktion unter Vorwärtswinkeln emittierten Deuteronen werden in der Strahlzeit im April 2000 erstmals zusammen mit dem Spectator-Aufbau in Betrieb gehen. Dabei erwarten wir, die ersten Spectator-Protonen nachzuweisen. Außerdem werden kurz die Schritte vorgestellt, die zur Erweiterung des Energiebereiches unter 6 MeV und zur Verbesserung der Akzeptanz des Systems nötig sind.

# Contents

# Chapter 1

# Spectator Protons at ANKE

Meson-production on a deuterium target motivates the detection of spectator protons at the ANKE experiment. The identification of the spectator protons is used to tag the reactions: pn→d$\omega$ and pn→d$\phi$ on the neutron of a deuterium target. A proposal to measure both reactions near threshold has been submitted by the ANKE collaboration and was accepted [2].

Therefore the results from simulations [5] on this type of reaction are briefly presented, concluding that one needs to detect deuterons with about 900 MeV kinetic energy under forward angles between 1° and 5°. and spectator protons in an energy range from 1.5 to 30 MeV under slight backward angles from 100° to 120°.

The setup of a spectator-detection system at ANKE not only opens the possibility to study such reactions on an effective neutron target, but also yields the possibility to determine the luminosity at ANKE in an energy range, where this has been previously impossible.

## 1.1 The ANKE Spectrometer at COSY-Jülich

The **Co**oler **Sy**ncrotron **COSY** at the Research-Centre Jülich can provide protons in an energy range from 45 MeV up to 2.7 GeV. A maximum of $4 \cdot 10^{10}$ protons per bunch has been accelerated up to now, and the first tests with a polarised beam yielded $2 \cdot 10^9$ protons per bunch (projected are $4 \cdot 10^9$ p/bunch).

The **A**pparatus for **N**uclear and **K**aon **E**jectiles **ANKE** is a magnetic spectrometer installed in the storage ring of COSY. The overlap with the proton beam is used for experiments on thin solid targets, a hydrogen- and a deuterium-cluster-jet target. A pellet target and a polarised-gas target are in preparation.

Ejectiles emitted under forward angles can be separated in the magnetic field of the main spectrometer magnet (D2). By the tracking in the multi-wire chambers, the emission angle and momentum of the particles can be accurately determined.

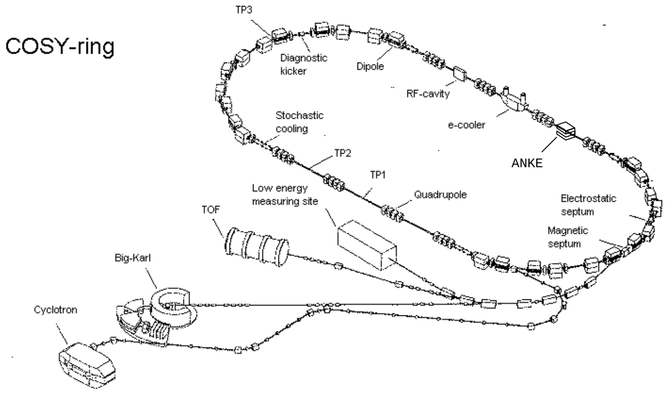


Figure 1.1: The Cooler Synchrotron COSY at the Research Centre Jülich

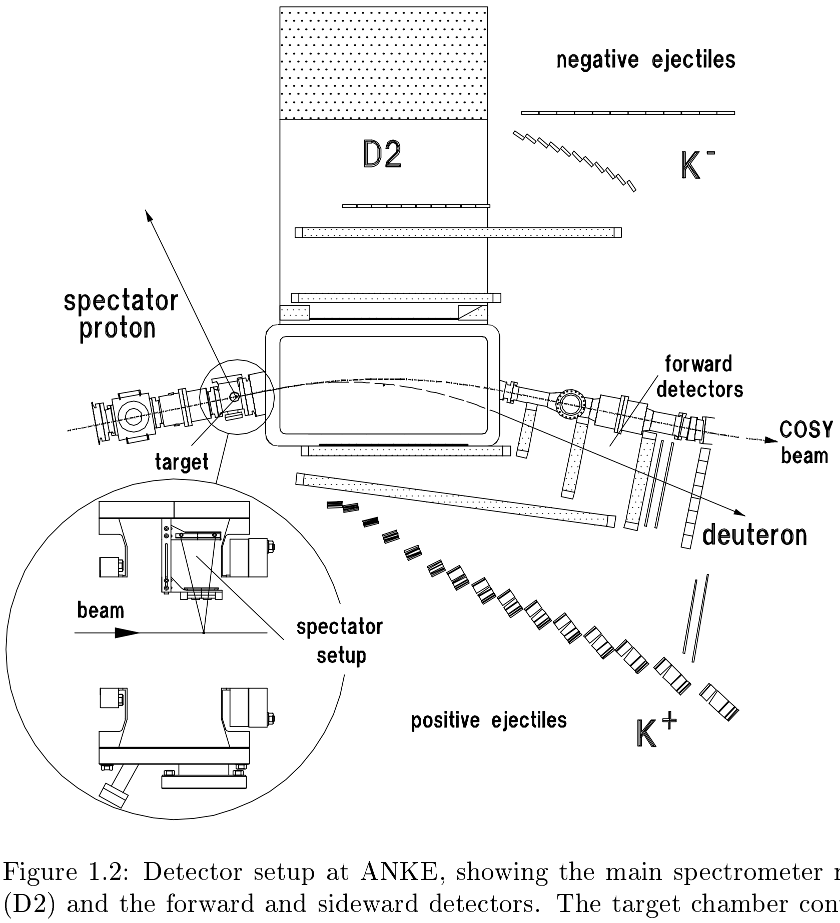


Figure 1.2: Detector setup at ANKE, showing the main spectrometer magnet (D2) and the forward and sideward detectors. The target chamber containing the spectator setup is shown in a magnified detail. The tracks from a deuteron in the forward detectors and a spectator proton are sketched.

**Side Detector Systems:** The detectors at the sides of the spectrometer have been optimised to track and identify kaons. Each side consists of two large wire chambers and two layers of scintillators for triggering and time of flight measurements. On the $K^+$-side the second scintillator layer is incorporated in 15 range telescopes in the focal plane of the magnet, which allow the identification of kaons out of a $10^6$ times higher background. Measurements on subthreshold $K^+$-production have been done and the results are currently analysed [9].

On the $K^-$-side, which is still under construction 11 specially curved Čerenkov counters should provide this identification. With the completed setup the correlated $K^+K^-$-production (e.g. from $\phi$ decay) is detectable with a high acceptance.

**Forward an Backward Detectors:** Three wire chambers for tracking and two layers of scintillators for timing are used for the forward detectors. Additionally eight Čerenkov counters have been set up under a small inclination angle, to be able to achieve an optimised particle identification at high momenta [11]. This setup covers forward angles from approximately 1° to 5° for deuterons with a momentum of $2\,\frac{\mathrm{GeV}}{\mathrm{c}}$ [10].

The backward detectors not shown in this figure allow the detection of the backward scattered proton in break-up experiments with the deuterium target.

**Spectator Setup:** The so-called "spectator setup" has been installed for the detection of spectator protons, which is the subject of this work and will be discussed in the following sections. It consists of three silicon detectors in a telescope structure mounted into the vacuum of the target chamber at ANKE. The setup can be used to detect low energetic particles, which have been emitted under large angles from the target. It is designed to cover an angular range from 83° to 103° and a proton energy range from 1.5 to 30 MeV (see chapter 2).

## 1.2 Spectator Protons for Meson Production

### 1.2.1 Physics Goals

In a certain energy range reactions can be done "quasi-free" on the individual nuclei of an extended nucleus. The remaining nuclei are not affected by this reaction and are left over as "spectators" with their intrinsic momentum. Thus the detection of the spectator proton from a reaction on a deuteron, enables us to tag the reaction on the neutron and to determine its intrinsic momentum, if the deuteron is known to be at rest[1].

This opens the large field of physics on the neutron for ANKE. For the ANKE spectrometer measurements of the $\omega$- and $\phi$-production on the neutron have been proposed [2] in order to study the following topics:

- **cross section for quasi-free $\omega$- and $\phi$-production on the neutron:** $\omega$-production cross sections in proton-proton collisions near threshold have been measured quite well. For pp→pp$\phi$ only scarce data is available. But the equivalent cross sections for the quasi-free reaction on the neutron

[1] The momentum of the nucleus in the used deuterium-cluster target can be neglected compared to the intrinsic momenta of the nucleons, caused by the Fermi motion.

have not yet been exploited. It is possible to study both reactions on a the proton and neutron from threshold up to 2.6 GeV.

- **intrinsic strangeness of the nucleon:** It has been suggested by Ellis et al. [4] that the ratio $R = \frac{\sigma(\phi)}{\sigma(\omega)}$ of these two cross sections at threshold depends on the intrinsic strangeness of the nucleon and the strangeness-production mechanisms. Assuming a deviation of 3.7° from the ideal $SU(3)_f$-mixing angle $\theta_i = 35.3°$ and the Okubo-Zweig-Iizuka (OZI-)rule [7, 18, 23] to be strictly valid, this value $R$ can be calculated to be $R = f \cdot 4.2 \cdot 10^{-3}$, where $f$ is the ratio of the phase-space factors of the two reactions. This obtained value differs considerably from some experimental results (up to $R = f \cdot (321 \pm 74) \cdot 10^{-3}$ [17]). Therefore the proposed measurements on the neutron promise a new aspect of the intrinsic $s\bar{s}$-component of the nucleon-wave function [4].
- **$\omega$N- and $\phi$N-elastic cross section:** Another interesting field is the elastic scattering of mesons on hadrons. This effect can be evaluated by the measurement of the high energetic (50 to 400 MeV) tail of the spectator-proton distribution.

A first step will be the measurement of the $\omega$-production. The first beam time is scheduled for end of 2000 or beginning of 2001. The cross section for the $\phi$-production is estimated to be a factor of 200 smaller than for the $\omega$-production [2]. Therefore a higher density pellet target, available not earlier than middle of 2001, has to be used. Thus only the forthcoming $\omega$-production measurement will be briefly described in this work.

### 1.2.2 $\omega$-Production on the Neutron

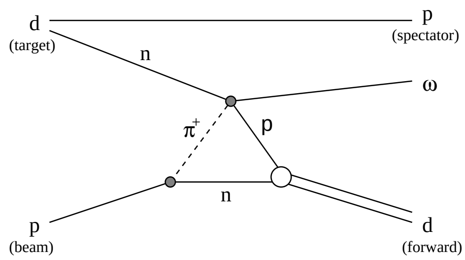


Figure 1.3: $\pi^+$-exchange as an $\omega$-production process in pd→ d$\omega$p$_{sp}$

The goal is to determine the cross section for the quasi-free reaction pn→d$\omega$ on the deuterium target. The cross section for the reaction pn→pn$\omega$ is significantly suppressed near threshold by the three-body phase space.

There are three particles in the exit channel of the reaction pd→ d$\omega$p$_{sp}$: a fast deuteron and an $\omega$ in forward and a slow ($T$ =0 to 30 MeV) spectator proton p$_{sp}$. These protons are distributed isotropically, if the the deuteron angle is not fixed[2].

The $\omega$-decay products: $\pi^+\pi^-\pi^0$ and $\pi^0\gamma$ are currently not completely detectable at ANKE. But if we determine the energy and azimuthal angle of the deuteron and the spectator proton, we can select the $\omega$-production reaction by the missing-mass method.

With the assumed dominating process of one-pion exchange for this reaction, simulations have been done for three different proton-beam energies [5] (As an example the $\pi^+$-exchange is sketched in figure 1.3):

[2] Near threshold intrinsic momenta antiparallel to the proton beam are favoured, and the spectator distribution is no longer isotropic.

- **1.8 GeV:** below the threshold for $\omega$-production on free protons (dashed line)
- **2.0 GeV:** compromising count rate and low angular momenta (solid line)
- **2.6 GeV:** at the threshold for $\phi$-production (dotted line)

Figures 1.4 and 1.5 show the momentum (or kinetic energy) and angular distribution of the deuteron and the spectator proton $p_{sp}$ in the exit channel of pd→ d$\omega p_{sp}$. The differential cross sections are plotted in arbitrary units and can not be compared for the different beam energies.

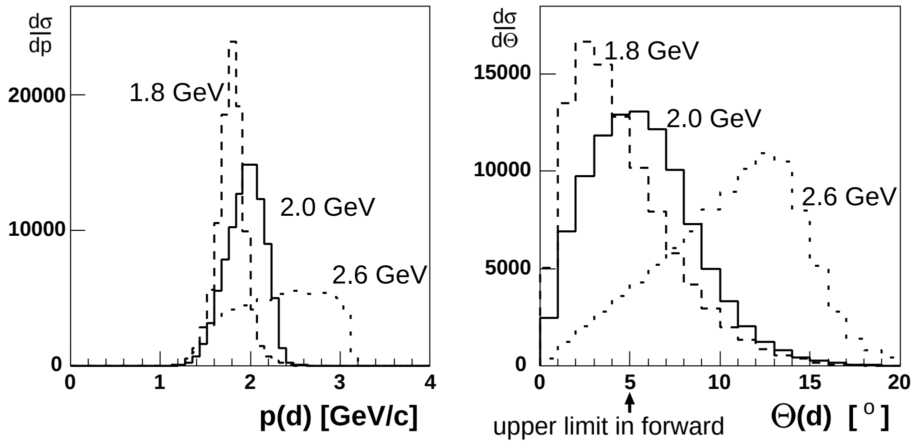


Figure 1.4: Simulated momentum and angular distributions of $\omega$-production for deuterons [5] (cross sections in arbitrary units)

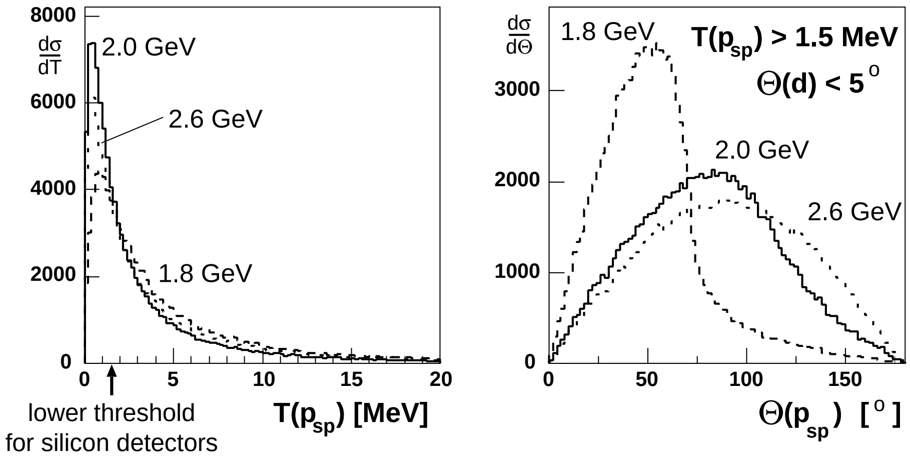


Figure 1.5: Energy distribution without cuts and angular distribution including cuts by simulations of $\omega$-production for spectator protons [5] (cross sections in arbitrary units)

The simulations curves in figure 1.4 already indicate, that the angular range of 1° to 5° for deuterons with 2 $\frac{\mathrm{GeV}}{\mathrm{c}}$ momentum with the forward detectors is satisfying our experimental needs.

The spectator proton energy range is a wide distribution which peaks between 1 and 2 MeV and has a long tail on the high energy side. We use the thinnest obtainable silicon detector with an active thickness of 18 $\mu$m in coincidence with the second layer, to suppress background and to identify the particles (see chapter 2). Therefore a lower threshold for spectator protons of 1.5 MeV has been estimated. Using this limit and the acceptance limit for the forward detectors at 5°, the angular distribution of the spectator protons has been simulated [5].

From the obtained angular distribution of the spectator protons (right in figure 1.5), angles between 30° and 120° seem reasonable for the spectator detection. As background significantly increases under forward angles and the identification of deuterons in forward direction is difficult because of their high momenta[3], simulations have been done including background reactions from $\eta$- and $\rho$-production as well as pd$\to$pX$p_{sp}$ for misidentified protons [2] (see also appendix C). Due to this an angular range from 100° to 120° is proposed for the detection of spectator protons.

The cross section for the $\omega$-production on the neutron has been estimated from the production reaction on the proton, measured at Saclay [3] to be 30 to 60 $\mu$b at 2 GeV beam energy [2]. Due to this rather large cross section, an experiment with a first setup yielding only a small acceptance for this reaction, can be used.

## 1.3 Luminosity

The knowledge of the luminosity is crucial for the measurement of any cross section. Therefore we designed our setup to allow such measurements. With the recently installed cluster-jet target there are no other means to determine the luminosity at ANKE with beam energies of 2 GeV or higher.

As cross sections for elastic scattering of protons on protons are very well known, we can use this process for the luminosity measurement. For beam energies higher than 2 GeV the second proton is outside the ANKE acceptance. On a hydrogen target we can use a single detected proton if we cut on an angular range of 70° to 90°. The cross sections from background reactions are negligible compared to the elastic scattering cross section. Similarly one can use the pd-elastic cross sections and detect the scattered deuteron on a deuterium target. Unfortunately only scarce data on the cross section are available in desired energy range up to 2.6 GeV. The measurement via quasi-free pp-elastic scattering is not feasible because of background and the missing acceptance in forward.

[3] According to publications from A. Kachavara et al. [11, 12] the protons can be suppressed by a factor between $10^{-2}$ and $10^{-3}$ using Čerenkov counters.

# Chapter 2

# Detection Concept

Having in mind the considerations discussed in the last chapter, we have to impose the following requirements on our spectator setup:

- **energy measurement** for protons in a range from the lowest possible energy ($\backsim$ 1.5 MeV) up to approximately 30 MeV with a resolution in the order of a few per cent,
- **particle identification** to separate protons, deuterons and background not originating from the target,
- determination of the **azimuthal angle** in an angular range covering backward angles for spectator protons with a resolution of less than 10°, additionally under forward angles for the luminosity measurement with elastically scattered deuterons with a resolution of a few degrees.

To fulfil these requirements in a single setup, we have chosen to use the sketched setup, which is briefly introduced here. We have arranged three silicon detectors in a telescope structure to cover an angular range from 83° to 104°. For a first setup we had to compromise the luminosity measurement and spectator detection.

- A **5 mm thick strip detector** has been used to stop protons with energies up to 30 MeV.
- Together with a **300 $\mu$m thick strip detector** the setup could be used for particle identification and tracking.
- A **18 $\mu$m thick surface-barrier detector** has been used to extend the energy range below 6 MeV proton energies.

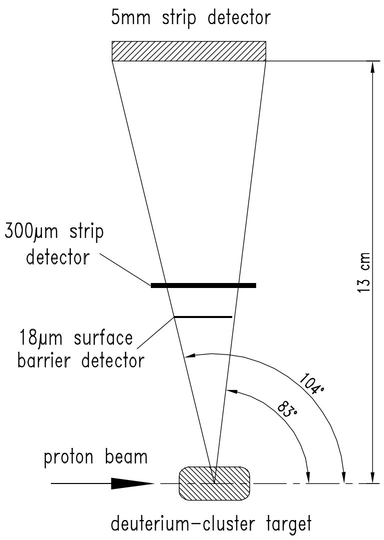


Figure 2.1: Schematic detector setup

The individual detectors are presented in appendix A. In the following sections the properties of this setup and the consequences for the possible ranges and resolutions are discussed in detail.

## 2.1 Use of Silicon Detectors

For our setup we used silicon detectors for the following reasons:

- **stopping power:** An accurate energy measurement together with the particle identification is only possible, if the particles will be stopped. At our institute thick lithium drifted silicon detectors have been developed to cover the whole projected energy range.
- **energy resolution:** Silicon semiconductors have an excellent energy resolution, low straggling and are easy to handle. Furthermore they can be produced with very thin entrance windows and are therefore ideally suited for the charged particle detection.
- **spacial resolution:** Silicon-strip detectors can be produced with a large variety in pitch and thickness (standard values are: thickness= $300\,\mu$m, pitch= $100\,\mu$m).
- **vacuum compatibility and full depletion:** These detectors can be produced to be vacuum compatible and sensitive over their full thickness (excluding dead layers of a few 100Å).

## 2.2 Energy Ranges

For particle identification and angular tracking the particles must penetrate a first layer and should be stopped[1] in the following layers. Considering only the stopping power of our detectors, we obtain the following energy ranges for the two $\Delta$E/E-combinations of our setup:

**18 $\mu$m and 300 $\mu$m thick detector**

| | |
|---|---|
| proton energy range | 1.2 to 6.2 MeV |
| deuteron energy range | 1.4 to 8.4 MeV |

**300 $\mu$m and 5 mm thick detector**

| | |
|---|---|
| proton energy range | 6.3 to 31 MeV |
| deuteron energy range | 8.5 to 42 MeV |

The shown minimum value is calculated by the punch through of the first layer(s) adding the detection threshold for the last detector. The maximum value corresponds to the stopping power of the whole detector combination.

These ranges are ideally suited to perform the spectator measurements, but the particle identification and the tracking described in the following sections restrict these ranges considerably.

[1] To obtain the required energy resolution the particles should deposit all their energy in the detectors.

## 2.3 ΔE/E-Particle Identification

**Bethe Bloch:** From the Bethe-Bloch formula [13] (see equation (2.1) below), it can be seen that the energy loss in matter depends on the charge $q = ze$ and the velocity $v$ of the incident particle. In the non-relativistic limit it is proportional to the square of the charge $q$ times the mass $m$ of the penetrating ion at a given kinetic energy $T$.

$$-\frac{dE}{dx} = \frac{4\pi e^4 z^2}{m_e v^2} NZ \left[\ln\frac{2m_e v^2}{I} - \ln\left(1 - \frac{v^2}{c^2}\right) - \frac{v^2}{c^2}\right] \xrightarrow{\frac{v}{c}\ll 1} \backsim \frac{mq^2}{T} \quad (2.1)$$

$N$ and $Z$ are number density and atomic number of the detector material (i.e. silicon) and $I$ is the average ionisation potential in this material.

**Particle Bands:** Therefore these energy losses are specific to the particle type, and we can use them to identify particles. If we do not have monoenergetic particles the difference can only be seen if the particles penetrate a first layer and are stopped in the second layer.

The particles can be distinguished if this energy loss is compared with the total energy of the particle. The expected energy losses in our detectors have been calculated, by integrating the linear stopping power (equation (2.1)) over the distance of penetration in the detectors. The deuteron band has only been calculated up to 29 MeV total energy - the kinematical limit at our setup.

Figure 2.2 shows the resulting curves in a plot of the energy loss in the first layer versus the energy loss in the second layer for both ΔE/E-combinations of the setup.

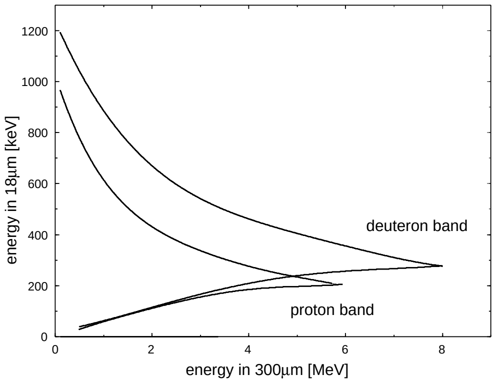


(a) 18 $\mu$m vs 300 $\mu$m

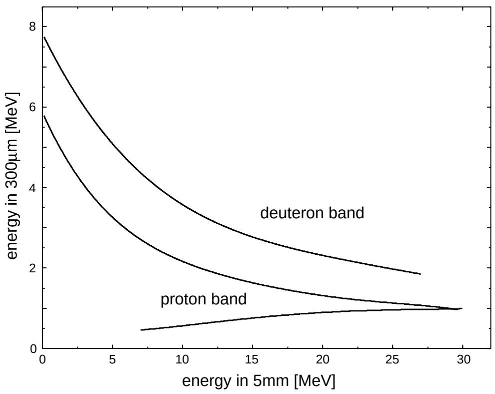


(b) 300 $\mu$m vs 5 mm

Figure 2.2: ΔE/E identification of protons and deuterons in the two detector combinations

**Band Overlap:** When particles also penetrate the second layer, it is possible that their band overlaps the band from lower energetic and lower Z particles stopped in the detector. The overlapping deuteron band in the first combination will restrict the energy range in which protons can be principally identified to a maximum of 4 MeV, if they can not be selected by kinematics or by the 3$^{rd}$ layer as a veto layer. In the second combination deuterons in this energy range were not present in our angular regime and therefore this restriction does not arise.

**Band Separation versus Resolution:** The ability to distinguish the particle bands depends on the separation of the bands and the energy resolution in the detectors. The resolution of the energy loss measurement depends in the first place on the intrinsic resolution of the detection system, i.e. from the detector itself and the electronic readout. Secondly it depends on the energy straggling in the first layer. As the energy loss is a statistical process, the part of the energy deposited in some penetrated layer is statistically distributed. Therefore the individual energy loss in each layer is affected by a statistical uncertainty, but not the total summed energy (if the particle is stopped in the setup).

| detector thickness | 18 $\mu$m | 300 $\mu$m | 5 mm |
|---|---|---|---|
| min. band separation | 150 keV | 800 keV | 4 MeV |
| detector resolution(fwhm) | 53 keV | 6 keV | $\leq$ 5 keV |
| energy straggling(fwhm) | 33 keV | 125 keV | — |

Table 2.1: Proton and deuteron separation in our setup

In table 2.1 the minimum band separation for protons and deuterons is shown in comparison with the energy resolution in the three detectors. For the detector resolution measured values given by the manufacturer are shown. With the knowledge, that additional noise from the electronic readout is not avoidable, we can conclude, that the separation of the particle bands for low energies in the 18 $\mu$m thick surface-barrier detector will be a difficult task. The energy straggling calculated by Monte-Carlo simulations [22] contributes considerably to the energy resolution, but can not be regarded as the limiting factor.

## 2.4 Tracking

It has been shown, that the azimuthal angle is needed for the meson-production measurement within 10° for spectator protons. For deuterons in a narrow energy range depending on the absolute angle this determination defines the accuracy of the luminosity measurement, and therefore an optimum should be found.

We have a proton beam with a diameter of approximately 2 cm, which is directed onto an extended deuterium-cluster target with a size of 7 mm perpendicular to the beam and 15 mm along the beam axis. Additionally the background rate in the target area at ANKE is expected to be high. This is due to the fact, that the cluster target produces rest gas in this area, and that high background rates have already been recorded from other measurements.

The spacial resolution in the 300 $\mu$m- and the 5 mm-strip detector, mainly determined by the pitch, can be chosen. In the following table the chosen distances between the strips and the total number of strips in the two detectors with spacial resolution are shown:

| | pitch | amount of strips |
|---|---|---|
| 300 $\mu$m detector | 1 mm | 32 |
| 5 mm detector | 235 $\mu$m | 200 |

Table 2.2: Chosen spacial resolution

With these dimensions and a distance of the detectors of 7 cm an angular resolution of 0.4° is obtained for particles with enough energy to neglect angular straggling. In the following paragraph it is shown that with this setup angular straggling is the main limitation to our tracking resolution.

**Angular Straggling** Particles penetrating a first detector before being stopped in a second one, not only lose a certain amount of energy in the first layer, but are also scattered out of their initial direction. This statistical process is called angular straggling.

Whereas the inelastic processes in charged particle interactions with matter are mostly responsible for their energy loss, the elastic scattering on nuclei is the main contribution for angular straggling of high energetic particles. The coulomb scattering is well described by the theory of Molière. In the limit of many small angle scatterings the following formula can be applied [20], called multiple scattering (MS):

$$\Theta_{MS} = \frac{13.6 \frac{MeV}{c}}{\beta p} \cdot Z \sqrt{\frac{x}{x_{rad}}} \cdot \left[ 1 + 0.038 \cdot \ln \left( \frac{x}{x_{rad}} \right) \right] \tag{2.2}$$

Where $\beta = \frac{v}{c}$, p, Z are momentum and atomic number, $x$, $x_{rad}$ thickness of the penetrated medium and radiation length in this medium.

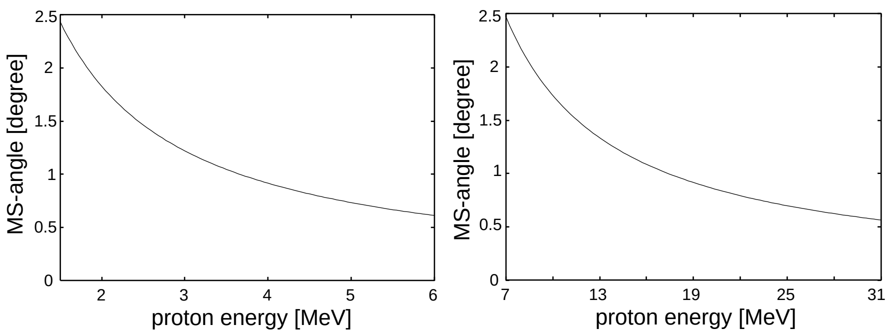


(a) 18 $\mu$m (b) 300 $\mu$m

Figure 2.3: Calculated curves for multiple scattering in the two penetrated detectors

The calculated straggling angles from multiple scattering alone are shown in figure 2.3 for both penetrated detectors in their projected energy range. From these calculations multiple scattering restricts our resolution to 2.5° for the following energy ranges in our setup[2]:

| $\Delta$E/E-combination | energy range |
|---|---|
| 18 $\mu$m and 300 $\mu$m | 1.5 to 6 MeV |
| 300 $\mu$m and 5 mm | 7 to 31 MeV |

As we obtained a angular resolution of 0.4° neglecting any straggling, we do not suffer any limitations in resolution from the pitch over the whole energy range (see figure 2.3).

As soon as particles loose a large fraction of their energy in the material, the inelastic processes become more significant, and the real straggling is underestimated by the curves in figure 2.3. It has been evaluated at our test beam time in Cologne (see chapter 3.6 on page 27), down to which energies equation (2.2) holds.

## 2.5 Conclusions

We have presented a setup which compromises the requirements for the measurement of spectator protons and deuterons from pd-elastic scattering. The ability to identify protons and deuterons and to determine the angle of protons within 2.5° has been proven in principle for a proton-energy range from 7 to 31 MeV.

Angular resolution can not be obtained by the 18 $\mu$m thick surface-barrier detector, used at this first beam time, but particle identification at proton energies from 1.2 to 4 MeV is principally feasible. It is also clear that this identification is at the limits of the detectors capability, because this detector has a high capacitance (i.e. noise) and the bands from protons and deuterons in the energy-loss spectra are not very far apart.

[2] Deuterons with 16 MeV have a corresponding angular straggling of about 2.5°.

# Chapter 3

# Detector Test at the Tandem Accelerator

The use of a 3 to 5 mm thick silicon-strip detector with a resistor-chain readout and an 18 $\mu$m thick surface-barrier detector[1] to detect protons, presents a non-standard task. Therefore a test under well defined conditions is important to study the properties of our system.

We took a first very similar version of the later used 5 mm thick micro-strip detector, a 300 $\mu$m thick surface-barrier detector and the 18 $\mu$m thick surface-barrier detector for our tests at the University of Cologne. The Tandem-Accelerator there provides a proton beam with the following properties, satisfying our requirements for this experiments.

- precisely defined proton energies in a range from 1 to 20 MeV
- a small and well defined beam shape
- only about $10^3$ protons per second on our detectors

The last point is crucial, because the beam intensity had to be reduced by many orders of magnitude compared with standard beam conditions. By a specially designed setup for this purpose and careful beam trimming these beam conditions could be achieved as desired.

In this chapter the accelerator, our setup with the detectors under test and how the required beam conditions have been achieved are described. Thereafter the individual measurements and their results are presented:

- The **reliability of the $\alpha$-calibration** has been checked by a comparison with the well known beam energy.
- The **spacial resolution** in the thick micro-strip detector has been evaluated with particles penetrating the detector perpendicular to its surface and under an inclination angle of 25° and 45°.
- **Angular straggling** in a penetrated $\Delta$E-detector has been measured and compared with the results obtained by multiple scattering calculations.

[1]The 18$\mu m$ detector is usually only used for fission fragments, which of course deposit much more energy in it.

- The crucial **energy resolution in the thin detector** has been studied for three different proton energies.

## 3.1 Cologne Tandem-Accelerator

The *Tandem-Accelerator* at the Institute for Nuclear Physics of the University of Cologne is able to accelerate many different nuclei in a potential of up to approximately 10 MV. Negatively charged ions are injected to the accelerator and stripped at the highest positive potential to be accelerated again on the exit side of the *Tandem*. This allows the acceleration of protons with energies up to 20 MeV. The demanded isotope is then selected by the magnetic field of a 90°-magnet, which is constantly measured with high accuracy. According to calibration measurements the energy of the accelerator can be determined within 0.2 per mille [16]. Without any special operating mode the selection can be assumed to yield an accuracy in particle energy of one per mille at least. After that the beam can be directed with an intensity of up to $10^{19}$ particles per second into different beam pipes with a large variety of experimental sites.

The position and focus of the beam is determined by scrapers and Faraday-cups, which can be moved into the beam pipe at various points and are read out with current-meters. Their sensitivity to a few pico amperes, implies, that more than $10^{10}$ protons per second have to hit any of these measuring devices to be detected and used for steering and focusing of the beam. This number is exceeding the maximum count rate of a few times $10^3$ particles per second, which our detectors and readout are able to cope with, by many orders of magnitude.

In the next chapter the setup, which has been designed with respect to this problem is presented. Thereafter the steps to achieve good beam conditions with this setup are described.

## 3.2 Setup

A first attempt, with a simple setup only using one collimator, a Faraday-Cup and a surface barrier detector to check the achieved beam conditions, did not yield satisfying conditions. The majority of the particles reaching our detector had been scattered before and thus lost some of their well defined initial energy.

Therefore we designed a completely new setup, which restricted the possible passage of protons to the optical axis of the accelerator. At the same time we provided the means to measure beam position and size at high intensities with this setup.

### 3.2.1 Collimator Setup

The collimator structure of our setup together with a Faraday cup behind, fulfilled the following tasks:

- to reduce intensity
- to confine the beam to a defined axis
- to restrict the acceptance for scattered particles

- to monitor the focus and position of the beam at high intensities

In figure 3.1 the collimator setup is sketched. Two almost identical groups with one collimator and two shielding plates have been mounted on a rod in a distance of about 25 cm. This rod could then be inserted in one peace into the beam pipe at the experimental site. We used an optical alignment system installed at this beam pipe to adjust the complete system exactly onto the beam axis.

**Confining the Beam:** Two collimators with an inner diameter of 3 mm and 1 mm have been used to confine the proton beam. These collimators have been fixed in centrosymmetric holders to provide the possibility of an exchange without any new alignment.

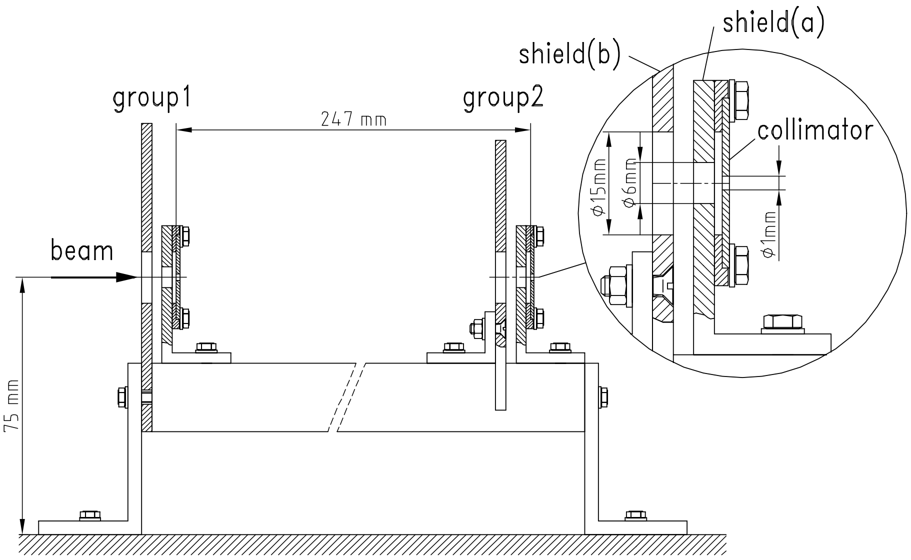


Figure 3.1: Collimator setup showing the 2$^{nd}$ collimator group as a magnified detail

**Monitoring the Beam:** To provide means to monitor the steering and focusing of the beam at high intensities, a current readout of four parts of the setup has been organised. As this is identical for both groups, only one is described. The collimator plate has been electrically insulated from common ground and was read out by a current meter. Additionally the acceptance has been reduced to a diameter of 6 mm by a shielding plate (a), also serving as a holder. This holder itself served as a second decoupled measuring device. A second shielding plate (b) restricted the acceptance for this beam-intensity measuring device to a diameter of 15 mm, and shielded our detectors from any scattered particles in the beam pipe.

With this current sensitive devices and a Faraday cup behind the setup, we could measure the beam position and focus at our setup. This provided a good tool to perform the first step of beam development at high intensities.

### 3.2.2 Detector Setup

Silicon detectors have been mounted behind the collimator setup serving the following purposes:

- final beam development with the so-called monitor detector, shielding the detectors under test at the same time
- supporting the strip detector in a way, that it can be moved and inclined with respect to the beam
- independent placement of ΔE-detectors in front of this strip detector, to be penetrated by the beam

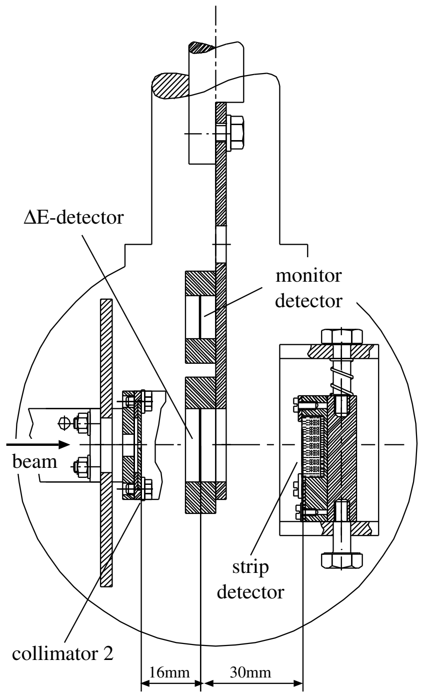


Figure 3.2: Side view of the detector setup in the target chamber

In figure 3.2 a side view of the setup in the used target chamber is shown. The proton beam passes collimator 2, having already transversed collimator 1 (see figure 3.1 on the preceding page).

A holder mounted on a vertical linear feed-trough gave us the possibility to direct the beam,

- into a monitor detector, stopping the protons afterwards in 3 mm of aluminium,
- through a ΔE-detector into the strip detector (shown position),
- or directly into the strip detector.

At last the protons are stopped in the thick strip detector, situated on a rotatable holder inside a U-profile. The whole profile is mounted on a linear feed-trough, providing a precise semiautomatic horizontal movement along the direction perpendicular to the sketched plane. Therefore two possible movements with the strip detector have been feasible:

- **Beam-scanning:** The above mentioned installation of the strip detector on the linear feed-through with a high precision[2] stepper motor enabled us to move it perpendicular to its strips and the beam. This could be used to study the position information from the detector.
- **Inclination against the beam-axis** has been prepared to yield five different angles relative to the beam: One position perpendicular to the detector surface and four positions inclined by $-25°$, $+25°$, $+45°$ and $+70°$. This could be used to show how the behaviour of the spatial resolution depends on the angle of the incident particle. (See chapter 3.5)

[2]An intrinsic precision of $0.5\mu$m has been provided by the motor itself.

In the following table 3.1 some of the properties of the three surface-barrier detectors from ORTEC and the thick lithium drifted strip detector are given. More details can be found in appendix A.

| detector | monitor | ΔE-detectors | | strip detector |
|---|---|---|---|---|
| active thickness | $372\,\mu$m | $18\,\mu$m | $300\,\mu$m | 3.0(1) mm |
| active area | $50\,\mathrm{mm}^2$ | $300\,\mathrm{mm}^2$ | $300\,\mathrm{mm}^2$ | $(10 \times 20)\,\mathrm{mm}^2$ |
| strips x pitch | — | — | — | 80 x $250\,\mu$m |

Table 3.1: Some properties of the detectors tested at Cologne

## 3.3 Beam Development

With all these tools we were able to perform the beam development in the following three steps:

- steering and focusing the beam at high intensities through a current sensitive collimator structure into a Faraday cup
- defocusing the beam with a quadrupole magnet just in front of the collimators, to reduce intensity to less than $10^{10}$ protons per second
- monitoring the final adjustment of the beam with a standard silicon detector, to achieve a stable and un-scattered beam with about $10^3$ protons per second

The important ratio of scattered versus un-scattered particles at our detector position can be easily evaluated from the energy spectra of our monitor detector. The finally achieved beam conditions are shown for a 6 MeV proton beam in figure 3.3.

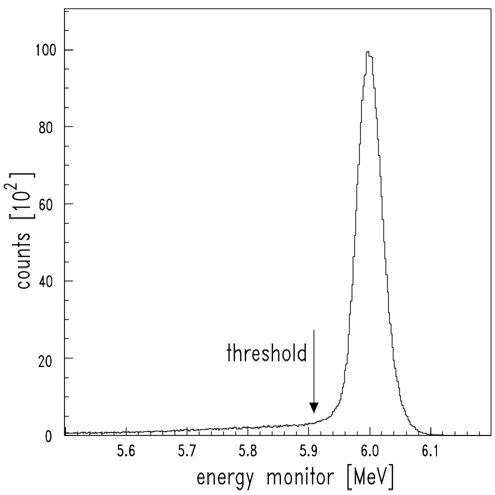


Figure 3.3: Beam energy distribution for a 6 MeV proton beam

A clean peak at 6 MeV beam energy[3] with a width of $\sigma = (21.86 \pm 0.04)$ keV has been observed. If we take the ratio of events with lower energies, than the threshold indicated in the figure, versus the events in the peak, we get a rough estimate of the amount of scattered particles. For this run a value of $(14 \pm 2)\%$ is obtained. Monitoring the beam online during the last step of beam development, we were able to achieve simular conditions for all beam energies.

[3]The energy calibration and comparison with the beam energies will be discussed in the next chapter.

## 3.4 Proton Energy vs $\alpha$-Calibration

As already mentioned, a good energy calibration is crucial for our experiments at ANKE. The precise energy of the proton beam at the Tandem accelerator, is ideal to check the reliability of the detector calibration.

In the following section the calibration with an $\alpha$-source is described, and thereafter the comparison with the energy deposit of the protons from the beam is discussed. This can be understood as a test on the energy deposit of $\alpha$-particles versus protons in silicon detectors as well as a check on the linearity of our system.

### 3.4.1 Calibration

The calibration of the detectors was done with an open alpha-source[4] containing three different alpha-emitters in a ratio with almost the same intensity of their strongest lines. In the surface barrier detectors we can still see the contribution from the less intense adjacent $\alpha$-peaks (see figure 3.4 on the facing page). Their intensity is about 20% of the corresponding main $\alpha$-lines.

| isotope | $^{239}Pu$ | $^{241}Am$ | $^{244}Cm$ |
|---|---|---|---|
| main $\alpha$-energy [keV] | 5157 | 5486 | 5805 |
| $2^{nd}$ $\alpha$-energy [keV] | 5144 | 5443 | 5763 |

Table 3.2: $\alpha$-energies of the calibration source used at Cologne

With these three points an energy calibration can be done, assuming that our system is linear over the used energy range. Pulse-hight defect corrections for energy losses in the dead layer(s) $\Delta E^{dead\ layer}$ and for nonionising contributions $\Delta E^{nonionising}$ in the active layer of the detector have been done [15] [8]. Since an open source was used, no corrections for any dead layers in the source itself had to be applied here. All energy losses where calculated with the program "SRIM" by J.F.Ziegler [22].

**Calibration of the Monitor- and 300 $\mu$m-detector:** Here $\alpha$-particles were stopped in the detector and deposited their residual energy completely in the detector. The energy-loss in the entrance window of these surface barrier detectors has been calculated from the specified[5] thickness of 800Å silicon equivalent. (see table A.1 on page 48)

The fit in the ADC-spectra has been done in PAW++ using six Gaussian peaks, corresponding to the tabulated $\alpha$-energies (see figure 3.4 on the facing page).

[4]Provided by the Institute of Nuclear Physics at the Cologne University; source number: ES 908

[5]Specifications by EG&G ORTEC

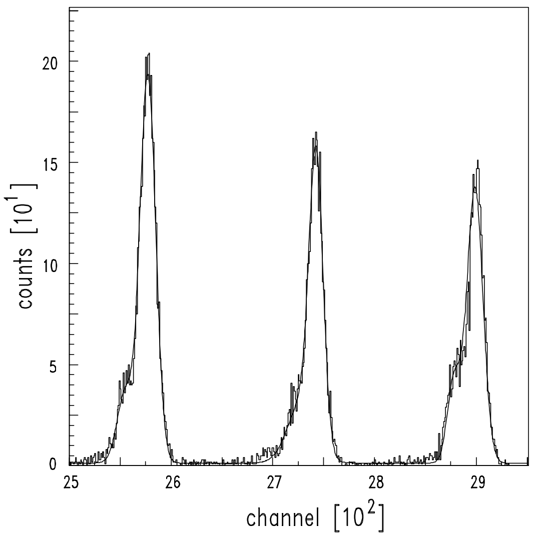


Figure 3.4: Spectrum and fit of a calibration with three main $\alpha$-lines and adjacent peaks

The deposited energy in the detector has then been calculated by:

$$E_\alpha^{yield} = E_\alpha^{source} - \Delta E_\alpha^{dead\ layer} - \Delta E_\alpha^{nonionising} \tag{3.1}$$

**Calibration of the 18 $\mu$m-Detector:** As $\alpha$-particles in our energy regime penetrate the detector, calibration is a slightly more tricky task. The simple solution to use a second calibrated detector behind this detector has not been possible with our setup. Thus we lead to rely on the specified depletion depth of the detector, and calibrated the detector using the calculated energy losses in this depletion zone. The as well calculated energy losses in the dead layer of course has to be subtracted from the $\alpha$-energy before the energy deposit in the depletion zone can be calculated.

$$E_\alpha^{yield} = \Delta(E_\alpha^{source} - \Delta E_\alpha^{dead\ layer})_{18\mu m} \tag{3.2}$$

Where $\Delta(...)_{18\mu m}$ is the deposited energy in a layer of 18 $\mu$m silicon by $\alpha$-particles with the energy given in brackets.

**Calibration of the Strip Detector:** We used a resistor chain readout for the 80 strips with 250 $\mu$m pitch, as described in chapter A.2 on page 48. A linear approach is made by the following considerations. By comparison with the beam energies, it could be shown (see chapter 3.4.2), that the response of our system is linear. We obtain an energy calibration from the sum of the two amplitudes:

$$E_\alpha^{yield} = E_1 + E_2 = slope_1 \cdot x_1 + offset_1 + slope_2 \cdot x_2 + offset_2 \tag{3.3}$$

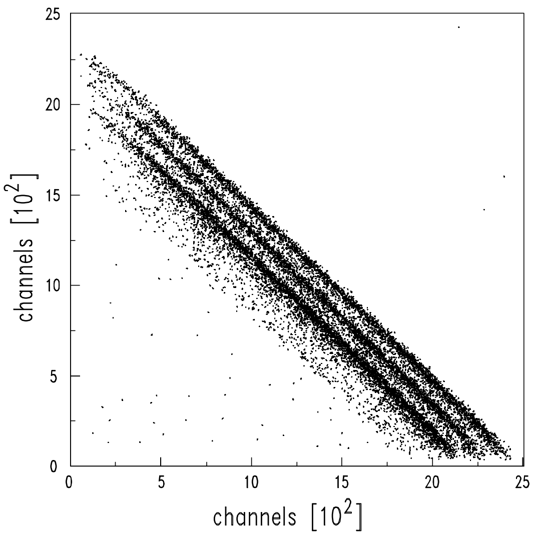


Figure 3.5: $\alpha$-lines in the two readout channels of the strip detector versus each other

with individually obtained ADC-values ($x_1$ and $x_2$ [channels]) for the corresponding $\alpha$-energy for each side of the resistor-chain readout and a common offset: $\mathit{offset}_1 + \mathit{offset}_2$. The relative position is then determined by the difference of the normalised amplitudes from both channels.

Plotting the two channels versus each other as shown in figure 3.5, a linear regression fit could be done for each $\alpha$-line. This can be used to get the ratio of one amplification versus the other. Proper sum spectra can then be created by rescaling one channel with this ratio as follows:

$$x_{sum} = \frac{slope_1}{slope_2} \cdot x_1 + x_2 \tag{3.4}$$

The generated sum spectra can then be calibrated by the simple linear approach as in the surface barrier detectors:

$$E_\alpha^{yield} = slope_2 \cdot x_{sum} + \mathit{offset}_{common} \tag{3.5}$$

Of course the deposited $\alpha$-energies $E_\alpha^{yield}$ were calculated in the same way from the energies of the source $E_\alpha^{source}$, as it was done in equation(3.1) for the surface barrier detectors. In this detector our front dead layer consisted of 0.1 $\mu$m aluminium plus 0.1 $\mu$m boron implanted silicon. (See also appendix A.2 on page 48)

**Proton Energy:** To calculate accurate proton energies from the $\alpha$-calibrated amplitude yield from the detectors $E_\alpha^{yield}$, of course the same corrections for pulse-height defects of protons have to be applied as for the $\alpha$-particles. An additional correction has been done, because according to W.N. Lennard [14] $\alpha$-particles produce about 1% more electron-hole pairs than protons of the same energy. Including all corrections the proton energy $E_p$ is then calculated as follows:

$$E_p = (1 + 0.01) \cdot E_\alpha^{yield} + \Delta E_p^{dead\ layer} + \Delta E_p^{nonionising} \tag{3.6}$$

The equivalent deposited $\alpha$-energy $E_\alpha^{yield}$ is the energy measured in the $\alpha$-calibrated system. The 1% difference in amplitude yield is taken into account by the factor of 1.01; and the losses due to dead layers and nonionising effects just have to be added. The resulting energy $E_p$ should then correspond to the initial proton energy.

### 3.4.2 Beam Energy

The deposited energy by the beam protons has been measured with the calibrated detectors. These values have then been re-calculated, as shown in equation (3.6) above to yield the initial proton energies. The results presented below, show the accuracy of our calibration and the linearity of the system.

**Monitor Detector:** Table 3.3 shows the results for the monitor detector:

| $E_{nom}$ | $E_{pred}$ [keV] | $E_{meas}$ [keV] | $E_{meas} - E_{pred}$ [keV] | $\frac{E_{meas}-E_{pred}}{E_{beam}}$ |
|---|---|---|---|---|
| 2 MeV | 1999.7±2.0 | 1997.9±60.4 | -1.8±62.4 | (-0.09±3.12)% |
| 2 MeV | 2000.2±2.0 | 1993.0±60.4 | -7.2±62.4 | (-0.36±3.12)% |
| 6 MeV | 6000±20 | 6063.6±92.3 | 63.6±112.3 | (1.06±1.87)% |
| 8 MeV | 4655±8 | 4668.4±81.3 | 13.5±89.3 | (0.17±1.92)% |
| 10 MeV | 3500±10 | 3472.6±72.0 | -27.2±82.0 | (-0.27±2.34)% |
| 15 MeV | 2347±15 | 2314.2±62.9 | -32.8±77.9 | (-0.22±3.32)% |
| 18 MeV | 2000±18 | 1965.2±60.2 | -31.9±78.2 | (-0.18±3.91)% |

Table 3.3: Check of the calibration with the beam energy in the monitor detector

The first column shows the nominal beam energy. The second column shows the predicted energy $E_{pred}$ to be measured in our detector. This value is calculated from the field of the 90°-magnet, which is used to measure the beam energy accurately. As soon as the protons were penetrating our detector (i.e. $E \geqq 8\,\mathrm{MeV}$) the calculated energy loss is shown here. Next the measured energies $E_{meas}$with errors including inaccuracies in the fit and the calibration are presented. Furthermore in the last two columns the deviations from the expected values are shown on absolute scale and relative to the particle energy $E_{beam}$.

Except for the result at 6 MeV incident proton beam all results are consistent with the expected values within approx. 30 keV. At 6 MeV unfortunately there is no value for the magnetic field. To compensate this we assumed a larger error than for the other energies.

This shows that the calibration with these three $\alpha$-lines is very accurate and the whole system is linear over the proton energy range of the $372\mu m$ thick monitor detector. Furthermore the energy loss calculation seem to be reliable too. This experimental results yield an accuracy on the per mille level[6].

**Strip Detector** In the table 3.4 on the next page the same properties are shown as for the strip detector, with the only difference, that the predicted energy always corresponds to the particle energy $E_{beam}$, because all protons are stopped in the detector.

[6]Assuming a slightly different beam energy as intended in the only run, where the exact value was not measured.

| $E_{nom}$ | $E_{beam}$ [keV] | $E_{meas}$ [keV] | $E_{meas} - E_{beam}$ [keV] | $\frac{E_{meas}-E_{beam}}{E_{beam}}$ |
|---|---|---|---|---|
| 2 MeV | 2000.2±2.0 | 1990±96 | -10±98 | (-0.49±4.90)% |
| 6 MeV | 6000±20 | 6136±139 | 136±159 | (2.22±2.66)% |
| 8 MeV | 7995±8 | 8073±165 | 78±173 | (0.97±2.16)% |
| 10 MeV | 9989±10 | 9982±190 | -7±200 | (-0.07±2.00)% |
| 15 MeV | 14992±15 | 15036±257 | 44±272 | (0.29±1.81)% |
| 18 MeV | 17987±18 | 17856±294 | -131±312 | (-0.74±1.73)% |

Table 3.4: Check of the calibration with the beam energy in the strip detector

The deviations of the measured values from the given beam energies are slightly larger than in the surface barrier detector. This fact and the greater error bars have two main reasons:

- A huge dynamic range had to be covered with this detector. $\alpha$-particles used for calibration were only available in a very narrow energy region between 5.1 and 5.8 MeV.
- The energy resolution of about 100 keV is approximately a factor of two worse than in the 372 $\mu$m thick detector.

Within the errors all the results coincide very well with the predicted ones. An accuracy in energy determination of less than 150 keV or 1% of the particle energy is not only a very good result over this large dynamic range, but is also fully satisfying our needs for the projected particle identification and luminosity determination at ANKE.

## 3.5 Spacial Detector Resolution

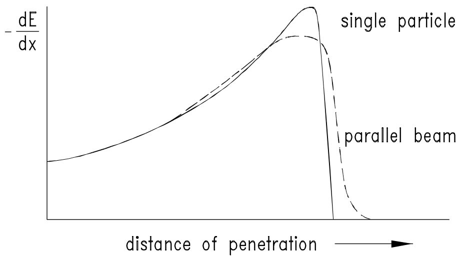


Figure 3.6: Bragg curve [13]: linear stopping power over the distance of penetration

Except from the obvious pitch size the distribution of the charge carriers produced by a single event, is also affecting the resolution. The shown Bragg curve for a single particle differs from the ionisation distribution of a parallel and monoenergetic particle beam due to statistical effects (i.e. straggling). This difference is too small to be evaluated at our experiment, but some effects due to the charge distribution from a single particle can be seen.

For perpendicular tracks the depth of the production of these charge carriers determines the position resolution due to diffusion (straggling is usually negligible). If the maximum diffusion is greater than pitch size, the averaging of the collected charges over a few strips can even lead to a better resolution, than without diffusion. Even with the 5 mm thick detector used at the ANKE-beam time the maximum diffusion has been calculated to be less than 70 $\mu$m, and therefore negligible compared to the pitch of 235 $\mu$m.

Our single sided strip detector with a pitch of 250 $\mu$m and an active thickness of 3 mm has been read out by a resistor chain (see appendix B.2). By taking the difference of the two read-out channels, the un-calibrated spacial distribution in our detector is obtained. The mean value of this distribution can then be taken as a beam position. Then the electronic resolution of course also affects the resolution. We checked this resolution and the linearity of the position determination in the following.

For inclined particle tracks the determined position of the incident particle and its resolution depends on the penetration depth at which the charge carriers are produced. The effect on the detector signal has been evaluated at the end of this section.

### 3.5.1 Perpendicular Tracks

**Beam Profile:** In figure 3.7 the spacial distribution of the events with a 15 MeV proton beam perpendicular to the surface of our strip detector is shown. The peak structure is corresponding to the strips with 250 $\mu$m pitch and the resolution of our resistor-chain readout.

With an infinite energy resolution, we would expect the following picture: A $\delta$-peak at each strip position neglecting charge splitting by hits in the gap between the strips. Including a finite energy resolution and charge splitting we expect a superposition of Gaussian peaks at the middle of the strips and a factor of ten smaller peaks in between[7].

If we apply this picture to figure 3.7, we can estimate a reliability to identify each strip of approximately $2\sigma$. This corresponds a resolution of $\sigma \approxeq 70\,\mu$m from the readout. This is better than the intrinsic detector resolution on the event basis, and therefore fully satisfying our needs.

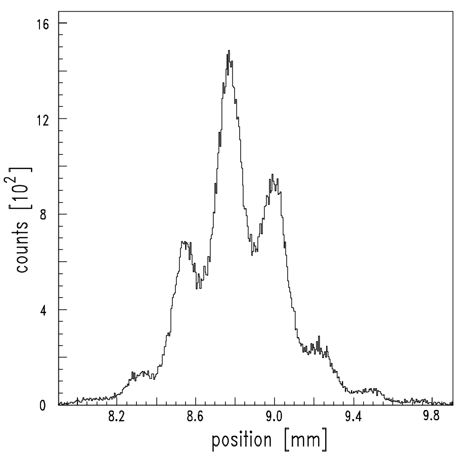


Figure 3.7: Spacial distribution of the beam obtained in the strip detector

**Beam Scanning:** We used the possibility to scan the beam precisely, by the movement of our detector with a stepper motor perpendicular to the beam. In figure 3.8 the raw difference in amplitude of the two ADC-channels is compared with the values from the linear feed-through for 18 positions at 15 MeV proton energy.

[7] The groove between the strips has ∽ 10 % of the width of the strips and the diffusion is only 7 $\mu$m for 15 MeV protons.

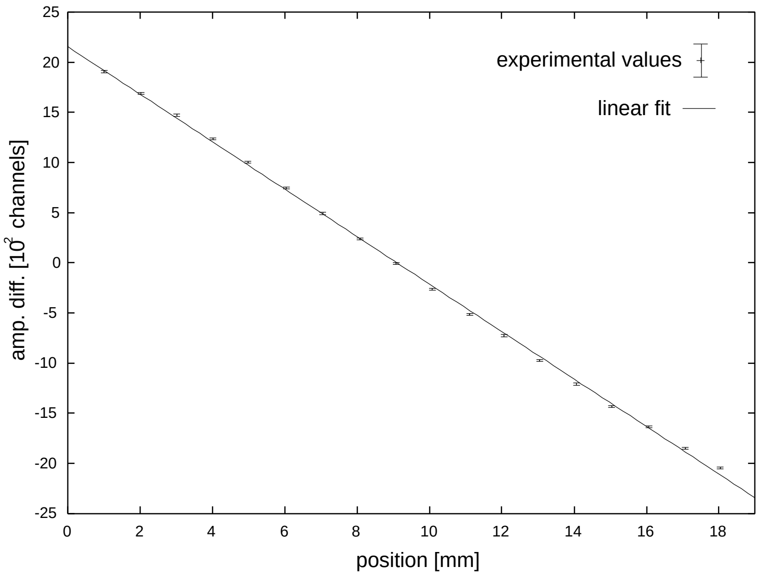


Figure 3.8: Amplitude difference of the two read-out channels versus the position of the stepper-motor readout

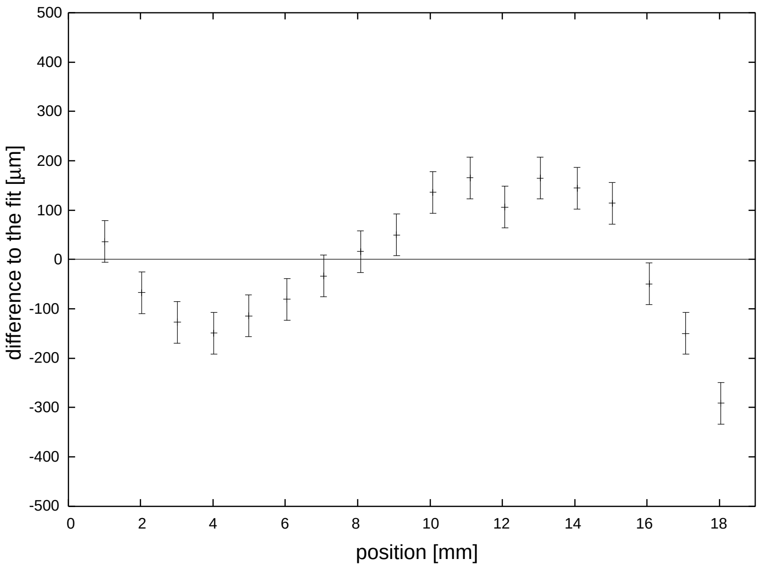


Figure 3.9: Difference of the calibrated experimental values and the linear fit versus the position of the stepper-motor readout

We can see that the linear approximation in figure 3.8 matches very well to the obtained values over the whole active size of the detector. Therefore we used this fit to do a spacial calibration of our detector and to calculate the deviations of these values from the fit. These values in figure 3.9 show some systematic dependence on the position, which obviously is due to an amplitude suppression in our electronic setup[8].

Due to this effect the relative position measurement across the detector can be determined within less than 300 $\mu$m. It is already clear from the values that the evaluation of a mean position with high statistics would be much more accurate, if this systematic effect could be excluded. Therefore different electronics including separate shaper fast amplifiers have been used at the ANKE-beam time.

On the other hand the position determination on the event basis with our setup can never be better than the distance between the strips (250 $\mu$m). It also has been shown in chapter 2, that a spacial determination of the particle tracks of 1 mm is sufficient for our purposes.

We can conclude, that the error in position for a single particle due to the differential method is of the order of the spacial resolution. Together with the needs for the experiment at ANKE, this does not require any further investigations.

### 3.5.2 Inclined Tracks

A particle transversing such a thick detector at an angle larger than a certain minimal angle, will yield charges on more than one strip. With a resistor-chain readout all the charges are integrated and will provide one single position value, which corresponds to the mean value of the ionisation distribution in the detector material (illustrated by the Bragg curve in chapter 2.4). These values will then be statistically distributed and will not peak at the individual strip positions.

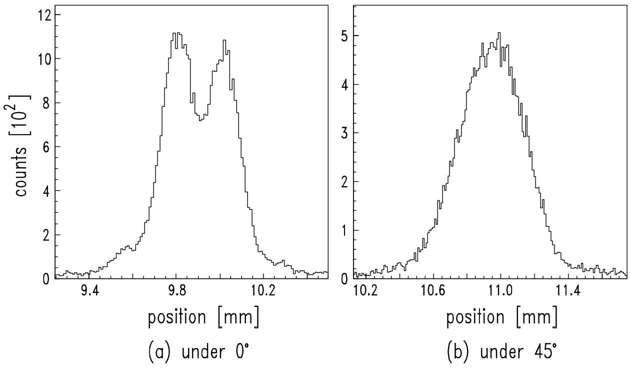


Figure 3.10: Beam profile with 10 MeV protons

In the experiment we have evaluated the behaviour of the spacial distributions at two different beam energies: 10 MeV and 18 MeV. In figure 3.10 and 3.11 the expected behaviour is seen. The strip structure appears, if protons penetrate the detector perpendicular (0°), but vanishes for the inclination of the detector.

[8]The timing due to trigger problems at high amplitudes seems to have been the reason.

As the change of angle had to be done by un-mounting the detector, the absolute position values are not comparable. Therefore the mean depth of the charge collection could not be evaluated.

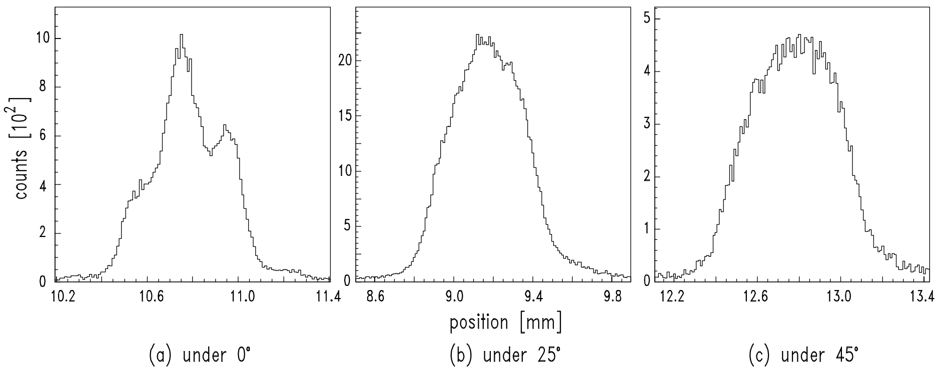


Figure 3.11: Beam profile with 18 MeV protons

With these facts we can estimate a minimum longitudinal spread of the Bragg distribution. If we do not see the strip structure anymore, the charge carriers have to be at least distributed over two strips for most positions. The minimum spread is then obtained using the pitch of 250 $\mu$m and subtracting the diffusion in the detector. It is calculated for the first angle, at which the strip structure vanishes. This corresponds to 25° at 18 MeV and 45° at 10 MeV[9] beam energy.

| | 10 MeV | 18 MeV |
|---|---|---|
| particle range | 710 $\mu$m | 2 mm |
| diffusion | 7 $\mu$m | 19 $\mu$m |
| min. spread | 344 $\mu$m | 547 $\mu$m |
| spread$_{50\%E}$ | 220 $\mu$m | 600 $\mu$m |

Table 3.5: Comparison of the obtained minimal spread of the charge carriers in our detector and an estimate from the Bragg distribution

To compare these values, we can calculate the spread of the charge carriers, which produce the last 50% of the ionisation before stopping. This value "spread$_{50\%E}$" shows that a significant part of the ionisation is spread over a larger distance than this value, because the Bragg distribution peaks at the end of the particle tracks.

A comparison of these values yields principal agreement, but the results are only boundary values and should be understood as a proof of principle.

[9] Unfortunately no measurement under 25° was made with 10 MeV protons

## 3.6 Angular Straggling

To evaluate angular straggling in a $\Delta$E-detector, we used the possibility to place the 18 $\mu$m- and the 300 $\mu$m-detector in front of our strip-detector. As already mentioned, at the ANKE-experiment angular straggling is crucial for the tracking resolution of our setup.

By checking the beam width with and without a first penetrated detector in comparison, we could calculate angular straggling and compare these values with the theoretical ones. To do these calculations we only need the following three experimental values:

- $\sigma_{direct}$: the sigma value corresponding to the width of the direct beam
- $\sigma_{penetrated}$: the sigma value corresponding to the width of the beam after penetration of a first $\Delta$E-detector
- $z_{\Delta E-E}$: the distance between the $\Delta$E-detector and the position sensitive detector

It has been assumed that the contributions to the width from the detector and the beam do not vary. I.e. the beam size is stable[10] and $\sigma_{det}$ is not energy dependent within a few hundred keV change in beam energy.

In the following the $\sigma$-values will be spacial values, and the angular values will be denoted with a bracket (i.e. $\sigma$ of the angle: $\sigma(\Theta)$) to distinguish them.

To calculate the spacial straggling $\sigma_{straggle}$, the measured beam width $\sigma_{penetrated}$ after the penetration of a first detector can be used:

$$\sigma_{penetrated} = \sqrt{\sigma^2_{direct} + \sigma^2_{straggle}} \tag{3.7}$$

With the distance $z_{\Delta E-E}$ of the first $\Delta$E-layer to the thick strip detector and the following relation, the angular straggling $\sigma(\Theta)_{straggle}$ can be obtained.

$$\sigma_{straggle} = z_{\Delta E-E} \cdot sin(\sigma(\Theta)_{straggle}) \tag{3.8}$$

$$\sigma(\Theta)^{exp}_{straggle} = arcsin\left(\frac{\sqrt{\sigma^2_{direct} - \sigma^2_{penetrated}}}{z_{\Delta E-E}}\right) \tag{3.9}$$

These experimental values are plotted in figure 3.12 and figure 3.13 on the next page. They can be compared with the theoretical curve, obtained by calculating multiple scattering with equation (2.2) in chapter 2.4 on page 11.

[10]Due to our beam limiting setup, we could observe this condition to be fulfilled.

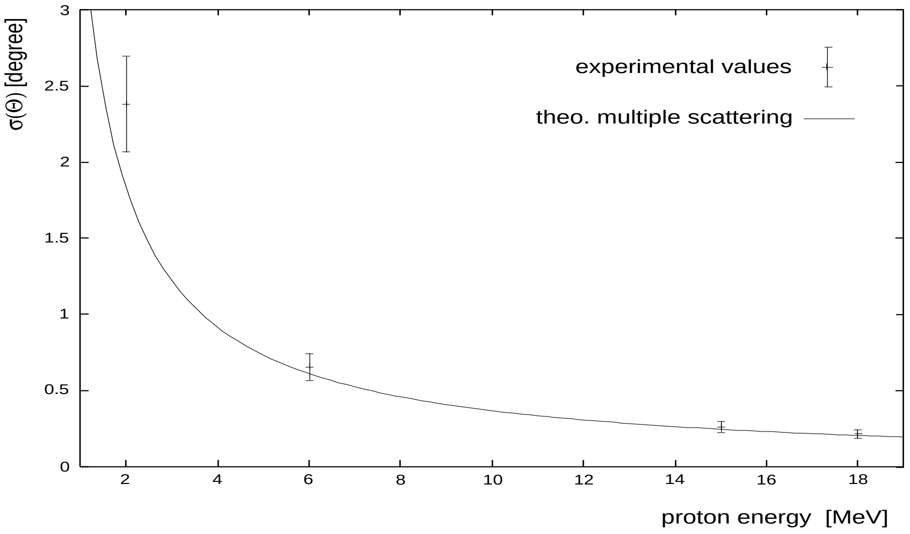


Figure 3.12: Straggling in the $18\mu m$-detector

We can clearly see, that this calculation only holds for small energy losses, i.e. high beam energies, where multiple scattering is the dominant effect. Slower particles lose greater fractions of their energy in one single interaction, and therefore the small angle scattering approach yields systematically too low straggling values, as it has been expected.

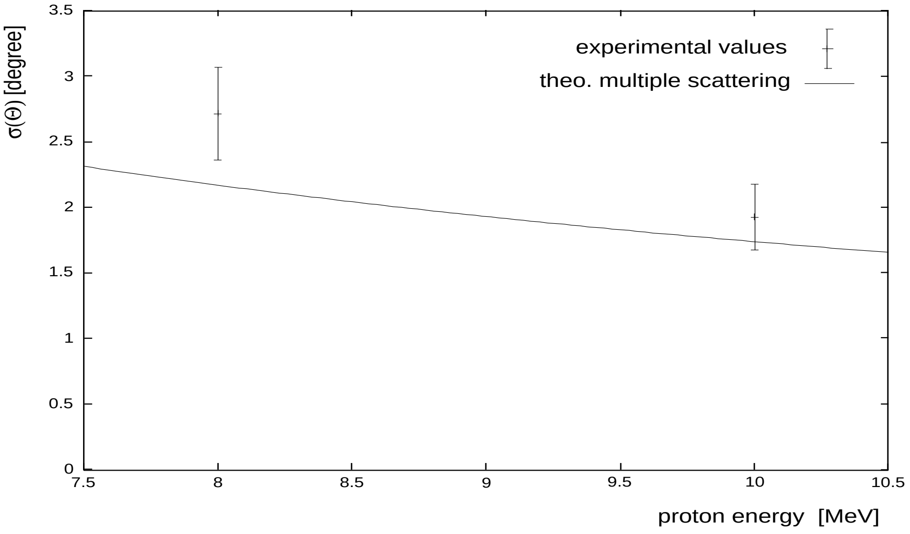


Figure 3.13: Straggling in the $300\mu m$-detector

We can therefore conclude, that measurements with an angular resolution of less than 3° are feasible down to an energy of 8 MeV including a $300\mu m$ thick penetrated layer.

## 3.7 Energy Resolution in the 18 $\mu$m-Detector

As shown in chapter 2.3 on page 9 particles can be identified by $\Delta$E/E-spectra by a combination of two silicon detectors. This is only possible, if the difference in energy loss in both detectors is greater than its energy resolution.

To check whether the separation of protons and deuterons is principally feasible in the 18 $\mu$m-300 $\mu$m detector combination, we evaluated the noise level and energy resolution in the thin detector. Figure 3.14 shows the energy resolution and noise level in the 18 $\mu$m-surface-barrier detector at different proton energies.

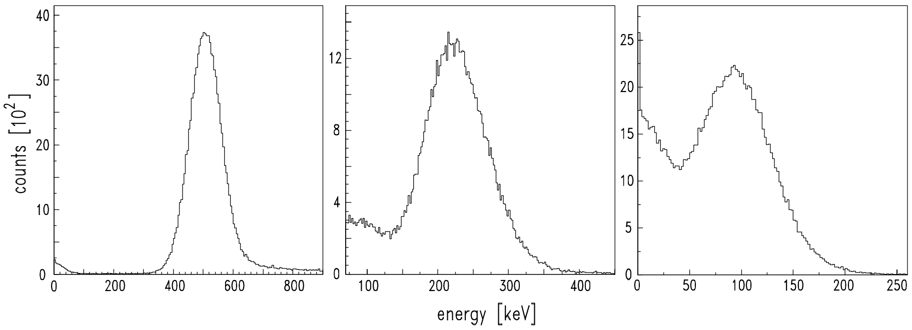


Figure 3.14: Energy resolution in the 18 $\mu$m detector

**Resolution:** From Gaussian fits to the proton peaks, an energy resolution $\sigma$ between 50 and 60 keV was obtained. This corresponds to a full width at half maximum of approximately 130 keV. Assuming a simular resolution for deuterons, this result implies a separation of protons and deuterons in a telescope structure of such an 18 $\mu$m thick detector and a second thicker detector with a confidence level of two sigma.

**Noise:** The evaluation of the spectra show, that about 10% of noise already is contributing to the proton peak at 6 MeV, whereas at 2 MeV the noise contribution is negligible. At 15 MeV proton energy the noise already represents approximately 50% of the peak. Although noise can be suppressed by coincidence with the second layer, results from protons at energies much higher than 6 MeV will certainly be obscured by this noise level.

## 3.8 Conclusions

With protons in the energy range of 2 to 18 MeV from the Tandem accelerator in Cologne the following results for the projected setup at ANKE have been evaluated:

- The energy of protons can be measured by the $\alpha$-calibrated strip detector within 1%.
- The position of a track in this detector can be determined within 300 $\mu$m.

- At the ANKE setup an angular resolution of less than $3°$ is feasible for proton energies higher than 8 MeV.
- The extension of the covered energy range down to 1.2 MeV is at the limits of the capability of the 18 $\mu$m thick surface-barrier detector.

This leads to the conclusion, that the combination of a 300 $\mu$m thick strip detector and the tested 3 mm thick micro-strip detector is able to fulfil the requirements for the spectator and luminosity measurements at ANKE. The crucial energy resolution in the 18 $\mu$m thick surface-barrier detector should be cross checked in the experiment.

# Chapter 4

# Experiment at ANKE

In September 1999 a measurement with 2 GeV protons on a deuterium-cluster-jet target was performed at the ANKE spectrometer of the COSY accelerator. From the previous considerations (see chapter 2) it is clear, that two tasks were required from our side, to do the projected measurements on meson production:

- determination of energy and azimuthal angle of the protons from the target
- measurement of the luminosity

By careful considerations on the design and placement of our detectors, we were able to fulfil both requirements with a single setup, which is described in the following section.

In an energy range from 7 to 30 MeV protons could be identified and their energy and angle was determined. The same could be done for deuterons from 9 MeV up to their kinematical limit of approximately 27 MeV[1]. Using these well separated deuterons, one can select the pd-elastic-scattering channel. The knowledge of the cross section of this reaction together with an accurate calibration yields the luminosity. This could not be measured before at this energy with the ANKE spectrometer.

A first attempt to cover an energy range down to 1.2 MeV with an 18 $\mu$m thick surface-barrier detector as a first layer is shown in chapter 4.4.

## 4.1 Setup

In chapter 2 the detector setup has been described in principle. In figure 4.1 on the next page the placement in the target chamber with the mechanical restrictions to the forward angles is shown. The four read-out segments of the 5 mm thick strip detector are indicated by numbers. The strips in the 2$^{\text{nd}}$ 300 $\mu$m thick detector are labelled in the same order (from right to left in the figure). Thus the position values obtained for both detectors follow the same systematics (ascending antiparallel to the beam direction).

Some properties of the three detectors used in the telescope structure are shown in the following table:

[1]Protons from 6.3 MeV and deuterons from 8.5 MeV upwards can be detected, but their angular resolution is poor due to straggling (s. chapter 3.6).

| | $1^{st}$ layer | $2^{nd}$ layer | $3^{rd}$ layer |
|---|---|---|---|
| thickness | $18\,\mu$m | $300\,\mu$m | 5.1 mm |
| pitch | — | 1 mm | $235\,\mu$m |
| number of strips | — | 32 | 200 |

Table 4.1: Properties of the detectors used in the setup at ANKE

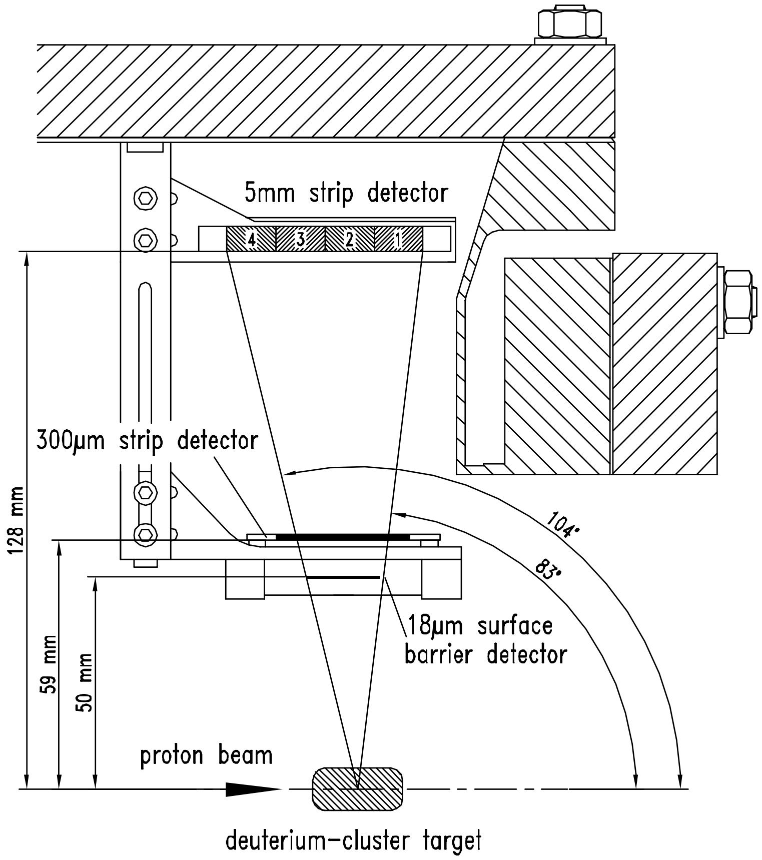


Figure 4.1: Detector setup in the target chamber of ANKE showing the incident proton beam from COSY overlapping the deuterium-cluster target and the three silicon detectors in a telescope structure, covering an angular range from 83° to 104°

## 4.2 Energy Calibration

The calibration has been done with an $\alpha$-source combined with a test pulser. By this method a good calibration could be achieved over the full energy range and the stability of the system could be monitored during the beam time.

After that the calibration has been checked by comparing the measured particle bands in $\Delta$E/E spectra with the calculated energy losses in the detectors.

### 4.2.1 Laboratory Calibration

A calibration of our setup was done in the laboratory before and after the beam time at the ANKE spectrometer with an $^{241}Am$ $\alpha$-source and a test pulser. This pulser provided signals with an amplitude, which is a selectable multiple of a fixed voltage. These signals are ac-coupled to the input of the preamplifiers[2]. Using this method we could check the following properties needed for a proper calibration:

- linearity of the whole electronic readout (and the detector for the thick micro-strip detector) using the test pulser,
- an accurate determination of the offset of each channel also by the use of the test pulser,
- a good determined slope of the calibration using the calibration point from the $\alpha$-source and the offset determined by pulser.

**18 $\mu$m-Surface-Barrier Detector:** Unfortunately no test pulser was used together with this detector. Therefore only a rough estimate on the offset could be done by the use of the pedestal peak. As $\alpha$-particles penetrated this thin detector, the calibration was done using the energy deposit in the 300 $\mu$m-strip detector to calculate the energy deposit in the 18 $\mu$m detector. As the energy losses of protons are much smaller ($\lesssim$ 1 MeV) than this calibration point ($\backsim$ 3 MeV), the uncertainty in the offset is strongly affecting our energy calibration. In figure 4.6 on page 41 systematic errors due to this calibration can be seen.

**300 $\mu$m-Strip Detector:** For the dynamic range needed for this detector, test pulsing yields deviations below 30 keV in linearity. The offset obtained by pulsing with a statistical error of 10 keV [3] can be used with the $\alpha$-energy for a calibration with an error of 2%

**5 mm-Micro-Strip Detector:** This detector was divided into 200 strips, which have been read out by four resistor chains in blocks of 50 strips (see chapter A.2 and B). As already mentioned the charge of the test pulser has been brought to the detector itself. Therefore the linearity and the offset of the complete system could be evaluated. A linear approximation of this dependence over the whole energy range corresponds to the pulser values within 100 keV.

Therefore the offset can be determined with an error of 50 keV. The calibration has then been done with the $\alpha$-energy as it has done at the beam time in Cologne (see chapter 3.4.1 on page 18) obtaining an error of approximately 2%.

### 4.2.2 Verification by the Experiment

**Pulser Check:** After the accurate calibration in the laboratory, our setup has been installed into the target chamber at ANKE. The only change, which has

[2]For our 5mm thick strip detector the charges have been injected onto the back side the detector, read out on the front strips. This method encloses nonlinearities due to detector response.

[3]The systematic error due to an intrinsic detector offset and nonlinearity is not known.

been made, was to install 25 metres of additional cable length between each preamplifier and the main amplifier in our detector readout. The attenuation in these cables has been calculated and measured in the laboratory. Additionally it has been checked at the experiment by repeating the pulser measurement from the laboratory. The attenuation in the cable from the pulser to the preamplifier was measured to be less than 0.3% and was neglected. These methods gave a value between 4 and 7% attenuation, which have been used to rescale the calibration. At the same time the use of this test pulser at the experiment, proved that our calibration has been stable during the beam time.

**Check with Energy Losses:** Another method to check the energy calibration, is to compare the measured energy losses at the beam time with values obtained by integration over specific energy losses [19] of particles transversing our detectors.

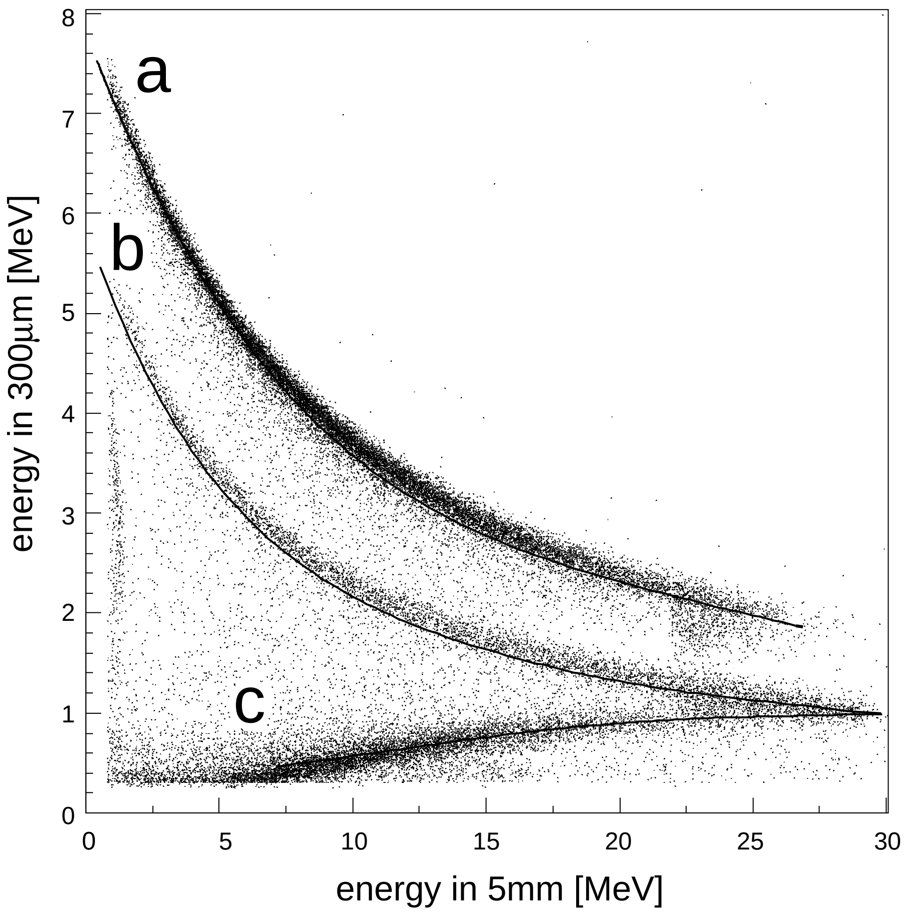


Figure 4.2: Comparison of calculated (lines) and measured (dots) energy deposits in the 300 $\mu$m and the 5 mm thick detector; a) deuteron line (all stopped), b) protons stopped in 5 mm, c) protons penetrating both detectors

For this comparison we can use the energy loss in the $2^{nd}$ detector versus the energy loss in the first segment of the $3^{rd}$ detector. In this plot[4] we can see the bands from protons over the full energy range (b) and (c), and the band from deuterons up to 29 MeV kinetic energy (a).

The calculated energy-loss curves plotted into figure 4.2 are consistent within 200 keV with the measured bands.

**Check with the Stopping Power:** We can compare the values from energy range curves [19] with the stopping power of our detectors. This latter value can be evaluated in this kind of spectra at the edge of the proton band (i.e. where curve (b) traverses (c)), where the highest energy deposit in the second detector occurred. This corresponds to particles, which just have been stopped in the detector. The same value can be obtained in this energy-loss spectra for the combination of the first two detectors. There we get the stopping power of deuterons and protons, if we roughly select either the forward or the backward angles with the strip detector (see figure 4.6 on page 41).

| | theoretical | measured |
|---|---|---|
| protons in 300 $\mu$m | 6.10(5) | 6.2(1) |
| deuterons in 300 $\mu$m | 8.05(5) | 8.1(2) |
| protons in 5100 $\mu$m | 30.2(3) | 29.5(6) |

Table 4.2: Stopping power of the detectors

The measured values all coincide with the theoretical values [19] within the errors. Therefore we can draw the conclusion that our energy calibration is right within its errors.

## 4.3 Luminosity Measurement

There have been no means to determine luminosity at 2 GeV proton-beam energy and the deuterium-cluster target up to now at ANKE. We selected pd-elastic scattering as a reaction with a known cross section at 2 GeV incident proton energy [6] and measured the scattered deuterons at large angles (close to 90° in our setup).

As there is no other process emitting deuterons in this angular regime with a significant cross section, it is sufficient to identify deuterons coming from the target, for the selection of this reaction. To be sure, it has been verified in a next step, that the selected deuterons obey the expected kinematical dependencies for pd-elastic scattering. The results with different beam intensities and a change in data acquisition prove that our setup is capable to yield the luminosity at ANKE with the deuterium-cluster target.

A further cross check with a rough estimate on luminosity by rescaling the results from another experiment, confirms our results. It also shows, that the gas pressures in the target can be used to rescale results on luminosity for experiments, where this value can not be determined directly.

[4]ANKE-beam time September 1999, 2 GeV protons on deuterium-cluster target, run1856

### 4.3.1 Background Suppression

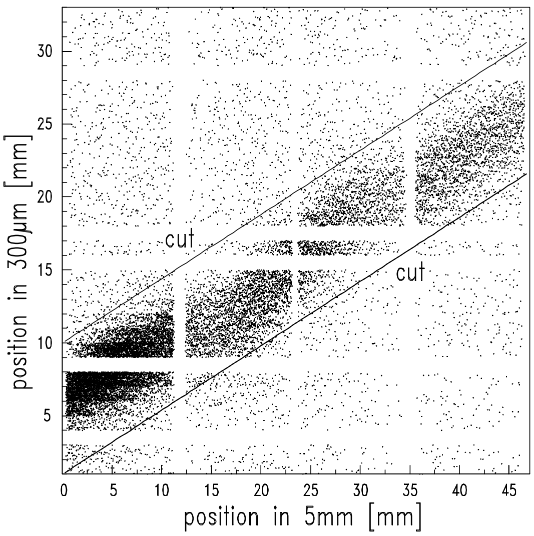


Figure 4.3: Plotting the spacial information from the 300 $\mu$m and 5 mm thick detector versus each other allows us to set cuts (lines) on the target region

The ability to determine the particle trajectory in the horizontal plane in the position sensitive detector layers, enabled us to suppress particles which have been scattered in the beam pipe or in the residual gas outside the target. In figure 4.3 the spacial information from the 300 $\mu$m detector[5] is plotted versus this information from the micro-strip detector. The forward angles correspond to low position values in both detectors.

The horizontal gaps are produced by the strips 3, 8, 15 and 17 in the 300 $\mu$m-strip detector, which were not working. The inefficiencies at the ends of each of the four segments from resistor-chain readout of the 5 mm-detector are responsible for the vertical gaps.

The width of the diagonal band corresponds to the target length along the beam axis of approximately 15 mm. The forward peaking due to elastic scattering, can also be seen by the higher count rate in the lower left corner of the plot.

The events outside this band (cuts indicated by the lines in the plot) correspond to the background rate of $(7.4 \pm 0.4)\%$ and can easily suppressed with this information. As there has been no spacial resolution in the vertical plane, background events differing only by these angles from the beam/target-overlap region can not be suppressed.

### 4.3.2 Deuteron Selection

In figure 4.4 the energy losses in the $2^{nd}$ layer are plotted versus the ones in the $3^{rd}$ layer in all four segments of the thickest detector. The band from the protons is seen over their whole energy range in all the segments. The band from the deuterons is only seen partially in the first and second segment. This is clear from kinematical reasons, because deuterons can not be scattered into backward angles. Because $83°$ is the minimal angle relative to the target, the maximum energy for deuterons in the first and second segment is restricted, which can be seen by the end of this band at about 27 MeV. The much worse resolution in segment 2 and 3 has been caused by an electrical shortcut in vacuum, and led to the decision not to use these segments for further data evaluation. To determine the luminosity, we selected the deuteron branch in segment one.

[5]The position in millimetres corresponds to the plotted strip number.

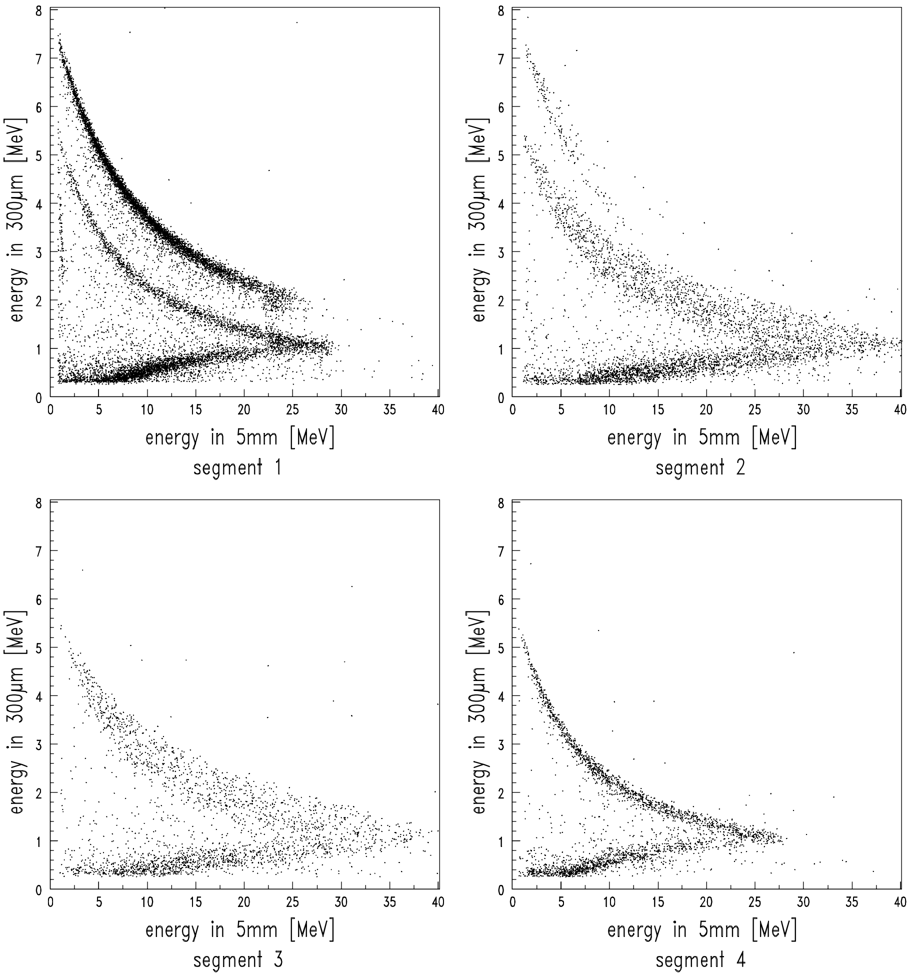


Figure 4.4: Particle identification using the energy losses in the 300 $\mu$m detector versus the losses in the four segments of the 5 mm thick detector

### 4.3.3 Proof of Principle

The above mentioned kinematical limit for deuterons from pd-elastic scattering can be evaluated more accurately by plotting the total energy deposit[6] of the selected deuterons versus their position in the last detector. Figure 4.5 shows this plot for the selected deuterons in segment number one.

The lower threshold of 8 MeV is caused by the stopping power of the two first detector layers. The efficiency of the electronic readout from a resistor chain sets a position dependent threshold, which causes the curved edges. The small band seen in the upper left corner, corresponds to electronic overflow (also bend due to the resistor-chain readout).

[6] The small contribution from the energy loss in the thin first layer has been neglected.

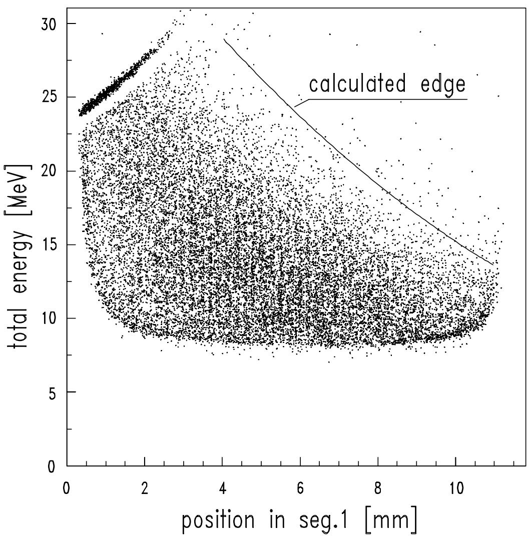


Figure 4.5: Kinematic limit for deuterons showing their total energy versus their position in the last layer

A clear edge can be seen from the upper left corner down to lower energies at the right side of the plot. This edge corresponds to the image of the target edge projected to our detector by kinematical limitations for deuterons from pd-elastic scattering.

This image of the target edge can be calculated using the dimensions of the setup and the target. These calculated curve, including multiple scattering in the penetrated layers and the energy loss in the $18\,\mu$m layer[7] is shown as a line in the plot.

The few events above this line prove, that the selected events are indeed mostly deuterons scattered elastically at our target.

The shift of this calculated line from the actual edge of the distribution shows a larger deviation than the uncertainty in the energy measurement, which has been cross checked before. The shift corresponds to a shift of the target edge of about 1.5 mm. For the determination of the luminosity (see next section) this uncertainty has been included in the error of the acceptance.

### 4.3.4 Luminosity Determination

After selecting deuterons from $\mathrm{pd}_{\mathrm{elastic}}$ we can use their count rate $R_d$ and the cross section for this process $\frac{d\sigma}{d\Omega}$ from [6] to calculate luminosity with the following equation:

$$L = R_d \cdot f_{dt} \cdot \left( \int_{\Delta\Omega} d\Omega \frac{d\sigma}{d\Omega} \right)^{-1} \tag{4.1}$$

**A dead-time factor** $f_{dt}$ has been included, to compensate losses in count rate by the dead time of the data-acquisition system. This value corresponds to the fraction of events, which have been accepted by the data-acquisition system versus the total triggered events. Intrinsic dead times from the detectors and trigger system have been on the per cent level compared to this value, and have therfore not been included.

[7] Due to a very high noise level in this detector, it has not been included in the summed total energy. This error has then been corrected for in the calculation of the image of the edge of the target.

**The rate $R_d$** of elastically scattered deuterons could principally be determined simply by counting all deuterons reaching our detectors. But in practice it is more feasible and accurate to cut on an appropriate energy range, where the calibration, energy losses, angular straggling, efficiency and cross section is very well known, and to evaluate the rate $R_d$ from this part. We used an energy range from 16 to 18 MeV for these reasons and because the variation of the cross section is minimal (i.e. minimising the error in $\frac{d\sigma}{d\Omega}$ due to our error in energy determination).

**The acceptance $\Delta\Omega$** bears the largest errors in our considerations, because this property depends strongly on the target size, position and beam overlap. In the horizontal direction the part of the target, which has been "seen" by our detectors, had to be rescaled to the total target size.

As shown in the previous section 4.3.3, these dimensions have rather large uncertainties. In the angular range used for our calculations the acceptance had been further restricted by the "dead" strip number 8 in the $300\mu m$ detector. The missing count rate for this dead millimetre could only be roughly estimated. We can just estimate the error from all these uncertainties in acceptance to be 15%.

**The cross section $\frac{d\sigma}{d\Omega}$** of pd-elastic scattering at a proton energy of 2 GeV is taken from [6]. For the small polar-angular range selected by the energy cuts, we can take the mean value of $\frac{d\sigma}{d\Omega} = (115 \pm 8)\frac{\text{mb}}{\text{sr}}$, because the systematic error of 7% is much bigger than the error produced by this averaging. Including an error due to the uncertainty in energy calibration, the total error of this value can be estimated to be about 10%.

The total cross section for the selected deuteron energy range in our setup is then: $\int_{\Delta\Omega} d\Omega \frac{d\sigma}{d\Omega} = (5.52 \pm 0.99) \cdot 10^{-30}\text{cm}^2$ with a relative error of 18%.

**Results** of five runs with a proton beam of 2 GeV kinetic energy are shown in the following table 4.3.

| run | $p$/bunch $[10^9]$ | $f_{dt}$ | rate $R_d$ [1/s] | **luminosity** $\left[\frac{10^{29}}{\text{cm}^2\cdot\text{s}}\right]$ |
|---|---|---|---|---|
| 1849 | 5.5(5) | 2.707 | 0.199(8) | **1.0(2)** |
| 1853 | 5.5(5) | 2.278 | 0.223(5) | **0.9(2)** |
| 1854 | 5.5(5) | 2.330 | 0.295(6) | **1.2(3)** |
| 1856 | 9.5(5) | 2.929 | 0.313(12) | **1.7(4)** |
| 1857 | 9.5(5) | 12.39 | 0.074(5) | **1.7(4)** |

Table 4.3: Results of the luminosity measurements with a 2 GeV proton beam

The dead time factor $f_{dt}$, the count rate of elastic scattered deuterons $R_d$ and the resulting luminosity is shown as well as the amount of protons per accelerated bunch in the synchrotron ($p$/bunch). This value corresponds roughly to the beam intensity, and can be used to compare relative luminosities. This only holds, if the beam overlap with the target and the target density did not change. The dead-time correction $f_{dt}$ is proven to be working, because a change in the dead time of or system changed the deuteron rate, but left the result on luminosity unchanged.

### 4.3.5 Rescaling Luminosity from another Experiment

A rough estimate on luminosity from pp$\rightarrow$d$\pi^+$ can be made using the values from a run at 500 MeV on a hydrogen-cluster target. The luminosity[8] was estimated by V. Koptev from the reaction pp$\rightarrow$d$\pi^+$ to be $(3.0 \pm 0.6) \cdot 10^{29} \frac{1}{\mathrm{cm}^2 \cdot \mathrm{s}}$.

From the gas-pressures in the cluster target we can estimate a ratio of densities from hydrogen to deuterium to be $\frac{\rho_\mathrm{H}}{\rho_\mathrm{D}} = 2.5 \pm 0.5$. Together with the given value of $(7.0 \pm 0.5) \cdot 10^9$ protons per injected bunch, we can rescale this luminosity to compare it with the measured values at our runs. We should keep in mind that this argument only works, if the beam-target overlap was the same at both experiments. The luminosity values obtained by this method are:

- **1.0(4)** $\cdot 10^{29} \frac{1}{\mathrm{cm}^2 \cdot \mathrm{s}}$ for run 1849 till 1854
- **1.7(6)** $\cdot 10^{29} \frac{1}{\mathrm{cm}^2 \cdot \mathrm{s}}$ for run 1856 and 1857

These values correspond nicely with our results but the reliability is low, because of their large errors. We can furthermore conclude, that the scaling with the target pressures seems to work quite well; and the beam-target overlap obviously did not change too much.

## 4.4 Spectator protons

The tagging of a spectator proton can only be done by the identification of a deuteron under forward angles. A forward detection system consisting of Čerenkov counters for the particle identification, wire chambers and two layers of scintillators will be installed at the ANKE spectrometer for the next beam time in April.

As the cross section for quasi-free pp-elastic scattering of a proton in our angular range is much higher than the one for meson production on the neutron, it is clear that no measurements of spectator protons could be done during this beam time. But the separation of protons coming from the target from deuterons and background is a very important requirement for these measurements, which could already be evaluated.

In the previous chapter 4.3 on page 35 it could be shown that this separation is indeed feasible with a high confidence level in the combination of the 300 $\mu$m thick 2$^{\mathrm{nd}}$ and 5 mm thick 3$^{\mathrm{rd}}$ detector layer. This corresponds to an approximate energy range of 6.3 to 31 MeV proton energy.

**Low Energy Protons:** We have seen in chapter 1 that the spectator proton distribution is peaked around 2 MeV. Therefore this separation would be important for the $\Delta$E/E combination of the 1$^{\mathrm{st}}$ and 2$^{\mathrm{nd}}$ layer. For this combination a proton energy range of 1.2 to 6.2 MeV is in principle accessible.

Two properties of the 18 $\mu$m thick 1$^{\mathrm{st}}$ layer make the situation for this combination very difficult:

[8] This luminosity determination can only be done with the hydrogen target and not at higher energies.

- no spacial resolution in this detector
- low energy deposit and high noise due to high capacitance

In the evaluation of background not originating from the target, we have seen that this ratio in comparison to the events from the target is in the order of a few per cent (see figure 4.3), and therefore the missing resolution should not prevent our measurements. But to do the meson-production measurement angular resolution is needed anyway; and therefore other detectors are already foreseen as a first layer (see chapter 5).

The reduction of the active area in the proposed pad detectors also helps us to reduce noise in this thin detectors, because the detector noise is proportional to the capacitance and thus to the active area of the detector. This high noise level not only inhibits the particle identification, if their energy deposit is very low, but also blurs the energy resolution at higher energy deposits.

In figure 4.6 two $\Delta$E/E-spectra from the combination of the 18 $\mu$m thick 1$^{\mathrm{st}}$ layer and the 300 $\mu$m thick 2$^{\mathrm{nd}}$ layer are shown. In figure (a) a coincidence of the particles leading to a signal above threshold in the first layer and the forward region of the second detector (i.e. strips 5 to 12) is shown. In figure (b) the backward region of the 300 $\mu$m detector is selected (i.e. strips 16 to 30).

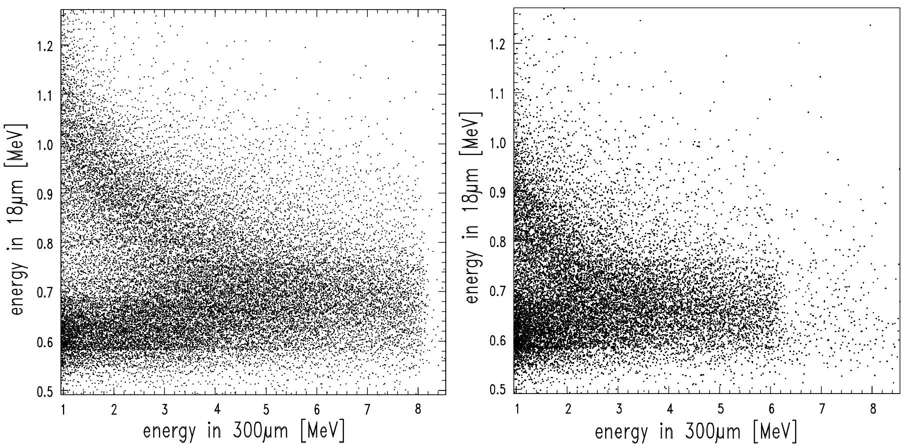


(a) forward direction (b) backward direction

Figure 4.6: Energy-loss spectra from the 18 $\mu$m versus the 300 $\mu$m thick detector

Even though the bands cannot be distinguished by themselves, it can be clearly seen that the deuterons with higher energy losses have vanished in the backward region (figure 4.6 (b)). As no pulser calibration could be obtained for the thin detector, the calibration in this 18 $\mu$m layer seems not to be very reliable; and a comparison with calculated energy losses would not be very helpful. In contrast to that, for the 300 $\mu$m detector a good calibration could be obtained. Thus the maximum energy loss of deuterons in the 300 $\mu$m detector of approximately 8 MeV can be seen in figure 4.6 (a) and the maximum energy loss for protons (6 MeV) limits the distribution under backward angels (figure (b)).

## 4.5 Conclusions

**Luminosity:** During the ANKE-beam time in September 1999 with 2 GeV protons on the deuterium-cluster target we were able to obtain:

- **the absolute luminosity within 18%**
- **the relative luminosity within few %**

The rather large error has two main reasons:

- Available data on the **cross-section of pd-elastic-scattering** is unfortunately scarce and not very accurate.
- The **shadowed target** implies large uncertainties, because we have to rely on dimensions, position and homogeneity of the target, to determine the luminosity.

Contrary to $pd_{elastic}$ the cross section from pp-elastic scattering is very well known over the whole energy range of COSY. Together with forward tracking and identification of protons at ANKE, our setup would be able to yield the luminosity by quasi-free pp-elastic scattering much more accurately than with pd-elastic scattering. Unfortunately the beam pipe restricted this setup to forward angles greater than 7°. Therefore we were not able to measure any coincidence with quasi-free pp-elastic scattering of this forward system with our setup at 2 GeV beam energy, and the separation of background (break up, $pd_{elasic}$, etc) could not be done.

In chapter 5 a setup is proposed, which would allow a much more accurate determination of the luminosity at all beam energies, combined with quite a few improvements for the proposed $\omega$- and $\phi$-production measurements. The question remains, weather we need higher accuracy on luminosity determination or not.

**Spectator Protons:** Parasitically we proved that our setup is ready to identify and trace protons in an energy range from 8 to 30 MeV at least, with the required energy and angular resolution for the measurement of meson production reactions on the neutron. (See also the discussion on angular straggling in chapter 3.6 on page 27.) The extension of this energy range to lower energies still seems to be a difficult task, but we were already able to see the different detector responses to protons and deuterons. We are hoping to solve these difficulties in a new setup (see chapter 5.2.1 below).

# Chapter 5

# Outlook

## 5.1 Beam Time in April 2000

The COSY-beam time in April 2000 is scheduled for the commissioning of the forward detectors with measurements on the break-up reaction: pd$\rightarrow$pnp at 500 MeV and 1 GeV beam energy at ANKE. The commissioning of the spectator setup can be done parasitically, with the following measurements:

### 5.1.1 Check of the Forward Detectors

A first check of the forward counters together with the spectator detection system can be done using pp-elastic scattering at 500 MeV beam energy. The following experimental work is proposed:

- **A proper coincidence** of the spectator and the forward detectors can be obtained by the coincidence from pp-elastic, which has a high cross section (i.e. count rate). This is essential for the tagging of the $\omega$-production out of a background which has at least $10^3$ times higher count rates.
- **The acceptance** of the whole setup can also be studied via pp-elastic scattering. Its accurate knowledge is important for the determination of any cross section.
- **In the Čerenkov counters a signal from a deuteron with $\beta$ =2.2 can be simulated** with a proton of 500 MeV. The crucial separation of protons and deuterons at a beam energy of 2 GeV can thus be experimentally evaluated by this measurement.

Due to the limitations in acceptance of the forward detection system, these tasks are not feasible at 2 GeV beam energy with the current setup.

### 5.1.2 Cross Check on Luminosity

We evaluated the luminosity from pd-elastic scattering at 2 GeV, where it could not be done by other means. A first hint has been given by pressure scaling of the target densities from another experiment at a different energy, that the assumed inaccuracies due to mechanical limitations may have been smaller than expected.

To check up to which extend we can minimise uncertainties from the target size and density distribution, we propose to cross check the luminosity measurements at 500 MeV beam energy in the April-beam time with the following reactions:

- pd-elastic scattering with the spectator detector only,
- pp-elastic quasi-free on the deuteron including the forward detectors,
- pp-elastic scattering also including the forward detectors,
- pp$\rightarrow$d$\pi^+$ with the well known acceptance for $\pi^+$ in ANKE.

The first two measurements can be done parasitically on the deuterium target and the latter two on the hydrogen target. By normalising the results with the gas pressures from the cluster-jet target, we can even compare all the four obtained values for the luminosity.

## 5.2 Next Steps

### 5.2.1 Spectator Protons below 6 MeV

It has been shown in chapter 2 that the identification of protons and deuterons is in principle possible with such a thin detector as a first layer. On the other hand, it has been shown, that the high noise level in the used 18 $\mu$m thick surface-barrier detector limits the particle identification to a low confidence level (see chapter 4.4).

The detector noise is mainly determined by its capacity, and therefore this quantity should be minimised. The reduction of the capacity of each read out segment or detector in the thin first layer of the spectator setup, implies the use of smaller active sizes or thicker detectors. The segmentation of the first layer will not only reduce noise, but also yield spacial resolution to suppress background and to determine the azimuthal angle of protons for the meson-production measurements with the extended cluster target.

It is difficult to achieve a segmentation in silicon detectors of this thickness, because larger pieces of 20 $\mu$m thick silicon are very difficult to handle. Two options are under discussion:

- **12 $\mu$m thick pad detectors** with a size of 1 cm$^2$ reduce the intrinsic noise by a a factor of about 2 and would yield a 10° angular resolution with a second layer 6 cm apart. The threshold for the identification of spectator protons would then be below 1 MeV.
- A **50 $\mu$m thick strip detector** can possibly be developed for our purposes with an optional pitch by Canberra. This should decrease noise and angular resolution to nearly any required value, setting the threshold for proton energies above 2 MeV.

Another option is the reduction of the thickness of the intermediate layer to 100 $\mu$m. From the results with 300 $\mu$m at the last beam time, we can assume that it should still be possible to cover the energy range up to 30 MeV with

$100\,\mu$m as a first layer. This setup would yield a lower threshold near 3 MeV proton energy.

A further tool to reduce noise in any silicon detector is cooling. As the thermal noise decreases proportional to $\sqrt{T}$ the noise could reduced by a factor of 1.5 for a temperature of $-150°$C. A cooling system is already planned, because the front-end chips, which will be used for the readout of the detectors, have to be operated in vacuum and have to be cooled anyway. Another advantage of cooling is, that the radiation damage can also be significantly reduced at lower operation temperatures.

### 5.2.2 Silicon Detectors under Forward Angles

A setup with x-y-sensitive silicon detectors at forward angles inside the vacuum chamber of the ANKE magnet is considered. Additionally the spectator setup should be extended to cover both sides of the target chamber.

In figure 5.1 the spectator setup covers large angles on both sides of the target chamber (left). Inside the vacuum chamber of the spectrometer magnet (D2) three layers of silicon detectors on both sides of the beam covering the forward angles are sketched. The COSY beam and two tracks from protons from pp-elastic scattering are shown.

Calculations on the optimised dimensions and positions for these detectors and the mechanical restrictions are analysed at the moment. First tests with double-sided silicon detectors and front-end readout electronics are currently performed at our institute.

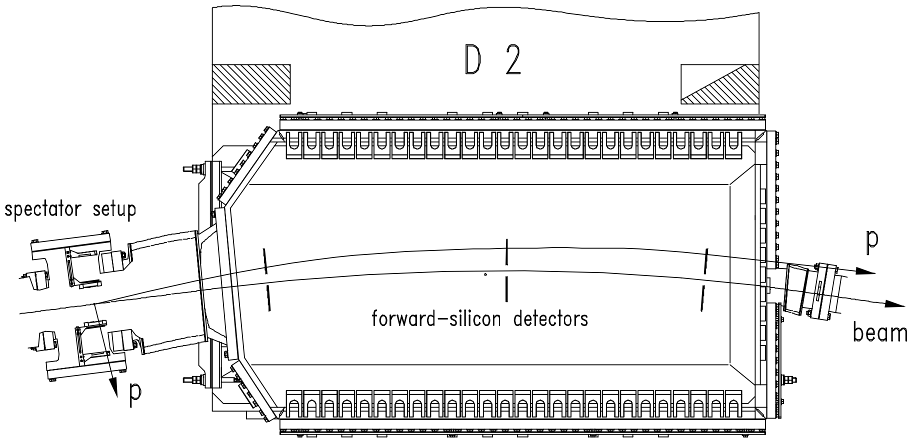


Figure 5.1: Proposed extended spectator setup in the target chamber (left) and forward detectors in the vacuum chamber of the spectrometer magnet (D2) from ANKE and two proton tracks from pp-elastic scattering

pp-elastic scattering can be used to calibrate this setup in energy and momentum and the following properties can be provided:

- The **acceptance** can be increased by a factor of two or more and to angles currently not accessible. The low cross sections of the $\omega$- and $\phi$-production make a high acceptance essential.

- The **momentum** can be measured with high accuracy by the determination of three points in the course of a particle in the magnetic field.
- The **luminosity** can be measured also on the deuterium target at all available beam energies using quasi-free scattering on the proton with a well known cross section.
- The **background** can be strongly suppressed by tracing the particles back to the target.

It can be stated that this proposed setup will be able to extend the capabilities of ANKE for $\omega$- and $\phi$-production measurements. This will be essential for the proposed measurements with a polarised beam and target, because of the significantly reduced luminosity.

# Appendix A

# Silicon Detectors

If particles transverse matter there is always a certain probability of interaction, and for charged particles there are two main processes:

- inelastic collisions with the atomic electrons of the material
- elastic scattering on nuclei

The first process contributes to the main part of the particle's energy loss. By collecting the charge carriers, the ionising part of this energy loss can be measured in semiconducting materials. The collection of light, produced by de-excitation in scintillators, is much faster, but a lot less efficient than this. The requirements on energy resolution, the restricted space in the ANKE target region and the handling in ultra high vacuum, let us choose silicon semiconductor detectors for our setup.

## A.1 Surface Barrier Detectors

Production is done, by exposing etched silicon to air yielding a very thin layer of silicon oxide. This is then covered with a layer of gold for ohmic contact and protection. A reversed bias voltage, applied to this contact and an indium contact on the back side (mostly covered by aluminium), creates a depleted layer just below this silicon oxide layer. Therefore surface barrier detectors are most suitable for the detection of low energetic and high Z particles. The commercial ORTEC detectors we used[1] (see table A.1 on the next page) had a dead layer of approximately $40\frac{\mu g}{cm^2}$ gold, which corresponds to an energy loss of only 8.9keV for a 5.5MeV $\alpha$-particle and 1.9keV for a 2MeV proton. The exit contact thickness was given to be: $40\frac{\mu g}{cm^2}$ aluminium Table A.1 on the following page lists some more properties.

[1] All specifications by EG&G ORTEC

| thickness | $18\mu m$ | $300\mu m$ |
|---|---|---|
| model no. | ED-095-300-25 | TE-020-300-300 |
| description | planar totally depleted | premium partially depleted |
| active area | $300mm^2$ | $300mm^2$ |
| si entr. window equ. | 800Å | 800Å |
| si exit window equ. | 2250Å | 2250Å |
| bias voltage | 10V | 120V |

Table A.1: Properties of surface barrier detectors

Neglecting any mechanical contributions (mounting, connectors, etc.), detector noise is proportional to it's capacitance, which is proportional to the active area and anti-proportional to the thickness of the depleted zone itself. From this fact we immediately realize, where noise is deemed to be our problem. - In the $18\mu m$-Detector. This is in fact a big challenge and has been evaluated at the test beam time in Cologne(see chapter 3.7 on page 29). Later at the ANKE beam time it was the reason for severe limitations (see chapter 4.4 on page 40).

## A.2 Silicon Strip Detectors

Due to this very thin oxide layer in the surface barrier detectors, the depletion zone cannot be extended very far into the silicon. Using ion implantation or diffused junction techniques, detectors can reach one or two millimetres depth of depleted zone and thus active detector thickness. By lithium drifting the density of the charge carriers in high purity silicon can be lowered even further, yielding the possibility to extend the depletion depth.

**Thick Strip Detectors from Mr Protić** :

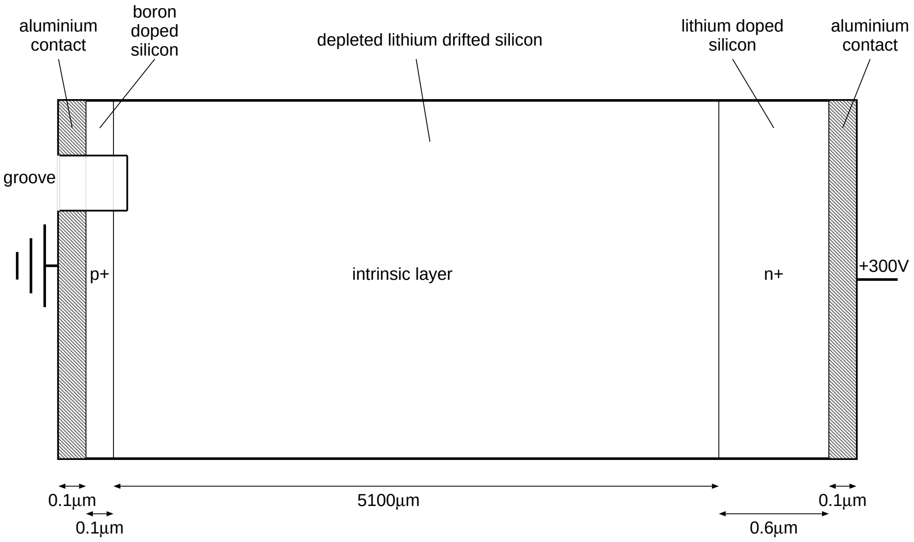


Figure A.1: Sketch of the thick strip-detector structure

For our purposes D.Protić developed five millimetre thick silicon detectors for us. These detectors are boron implanted from one side, and from the other lithium is thermally diffused into the detector at 350°C. The boron doped p+ layer with a thickness of $0.1\mu m$ is coated by $0.1\mu m$ aluminium and represents the entrance window of this detector. This corresponds to an energy loss of approximately 30keV for 5MeV alpha particles and 3.3keV for 2MeV protons. On the back side the lithium doped layer is between 0.5 and $0.7\mu m$ thick and also coated with aluminium for ohmic contact to the bias voltage. Lithium of this layer has been drifted into the pure silicon by applying a strong reverse bias voltage at 60°C, to compensate for traces of boron acceptors in the highly pure silicon. In figure A.1 on the preceding page a cut through the detector is sketched showing also one representative groove between the strips.

These detectors are divided into strips of $250\mu m$ respectively $234\mu m$ pitch, with a guard-ring surrounding the active area. The first type has been used at the test beam time in Cologne and in another setup previously installed at ANKE. The latter type performed very well in the latest ANKE beam time, providing us with data to determine luminosity at ANKE. (See chapter 4.3 on page 35) Resistor chain readout was used on both types, but on the latter type the resistor chain was subdivided to achieve an acceptable dynamic range with a total of 200 strips. Table A.2 shows some properties of these detectors.

| | # 1 | # 2 |
|---|---|---|
| pitch | $250\mu m$ | $234\mu m$ |
| groove width x depth | $27(5)\mu m$ x $1.5\mu m$ | $23\mu m$ x $4\mu m$ |
| depletion depth | 3.0(1) | 5.1(1)mm |
| bias voltage | from 300V up to 500V | |
| active area (l x w) | 10mm x 20mm | 46.8mm x 23mm |
| strips x groups | 80 x 1 | 50 x 4 |

Table A.2: Properties of the thick strip detectors

Detector number 1 was used at the test-beam time in Cologne and number 2 in the beam time in September 1999 at ANKE.

The large depletion zone makes drift times and diffusion relevant for discussion. The drift time for charge carriers sets direct constraints for electronic settings, and can lead to wrong conclusions, if not properly taken into account. Electron-hole pairs from particles, being stopped very close to the surface of the detector, create a fast signal from the positive charge carriers, and thus yield a good position resolution as diffusion is small. The drift time of the electrons then reaches it's maximum value. For higher energetic or lighter particles, which are stopped near the end of the detector, the drift time and the diffusion of the holes becomes maximal and therefore charges from a single hit gain their maximal spread in position at the strips. For minimum ionising particles, which deposit their charge almost evenly over the hole detector, the maximum spread in charge collection time is reached.

Table A.3 on the following page shows some values for this detectors, which were obtained in two different ways. For electrons the velocity was extracted out of curves from Bertolini and Coche [1]. And for holes they were calculated by $v = \frac{s}{t} = \mu E$ with the mobility $\mu_h = 480\frac{cm^2}{Vs}$ for holes and $\mu_h = 1350\frac{cm^2}{Vs}$

for electrons [21] , assuming the velocities to be far away from threshold and definitely gaining a maximum value by this method.[2] The diffusion is obtained then by: $\sigma_{diff} = \sqrt{2Dt}$ with diffusion constants calculated from the mobility. As the velocity at this field strength is still linearly dependent on the electric field, it is obvious, that the diffusion does not depend on the charge carriers.

| | electrons | holes |
|---|---|---|
| velocity $[\frac{cm}{s}]$ | $8 \cdot 10^5$ | $2.8 \cdot 10^5$ |
| max. drift time | $640ns$ | $1.8\mu s$ |
| diffusion constant | $34.6\frac{cm^2}{s}$ | $12.3\frac{cm^2}{s}$ |
| max. diffusion $\sigma$ | $67\mu m$ | $67\mu m$ |

Table A.3: Maximum diffusion and drift times in the 5 mm thick detector

As we can see in table A.3 the charge collection time due to drift time can be quite long, and should therefore be carefully considered. One disadvantage of the large integration times used to cope with the long charge collection times, is clearly the limitation in count rate imposed by it. The estimated pile-up can clearly be seen in the data obtained at the test beam time with the Tandem Accelerator. (See chapter 3.1 on page 14) The full width half maximum of the diffusion is mostly less than $100\mu m$, and therefore does not change the position resolution considerably.[3]

**Canberra Detector** In our later setup at the ANKE spectrometer we used a $300\mu m$ strip detector, commercially available from Canberra, as an angular sensitive intermediate layer between the $18\mu m$- and the thick detector. The front surface of this "Passivated Implanted Planar Silicon (PIPS) Detector" is ion-implanted and passivated instead of coated by an evaporated metallic layer. Due to Canberra this considerably reduces the entrance window thickness. This and other specifications given by Canberra are listed in table A.4.

| | Canberra Detector |
|---|---|
| model no. | PF-32CD-15*32-300-EB |
| thickness | $300\mu m$ |
| active area (l x w) | 32mm x 15mm |
| si entr. window equ. | <500Å |
| pitch | 1mm |
| strips | 32 |
| bias voltage | 20V |

Table A.4: Properties of Canberra $300\mu m$ strip detector

[2] The minimum bias voltage was used to gain upper limits.

[3] A slight change in the beam profile due to this effect could be seen in the data from the Cologne test beam time, but the evidence is too weak to be stated here.

# Appendix B

# Signal Processing

## B.1 Shaping and Dynamic Range

Main goal for the read out electronics is the amplification of by comparison small deposited charges in the silicon detector to a signal, with a reasonable amplitude for the analysis in a multichannel analyser (typically $\lessapprox 10$V). This voltage should be proportional to the deposited charge over the whole range of charges, which are to be analysed. Concurrently all contributions by stray fields, leakage currents and other detector noise, should be dismissed as far as possible, keeping the electronic noise itself minimal.

Taking into account all this, a readout chain for our silicon detectors is set up as follows: A charge sensitive preamplifier is installed as close to the detector as possible, to reduce the input capacitance and therefore the noise produced on the very sensitive input side. The signal is amplified again in the main amplifier(s), which provide(s) adjustable amplification, shaping and pole zero correction, to be then transmitted to an analyser, which produces a channel number corresponding to the amplitude of the signal, only if the trigger tagged it as an event. Amplification should be adjusted, to cover the amplitude range of the multichannel analyser and a correct pole zero adjustment ensures a charge proportional pulse height.

**Shaping** To ensure complete charge collection, decay times from the pre-amplifiers are usually quite long, so that the fast following signals will overlap with these and the amplitude will not represent the individual deposited charge anymore. Because the fast rising slope from the signal contains the basic information on the charge, differentiation is done with RC-networks. Therefore the system can yield a good measure of this charge even for high count-rates. The sharp differentiated signal is difficult to process and contains all high-frequency components of any noise produced in the system. Subsequent integration of the signal is often done in many steps by CR-networks, to produce a nearly Gaussian shape of the signal, which minimises noise and can be well processed by channel analysers. Another approach is to integrate and differentiate after the first differentiation again. The yielded fast bipolar signal can be used for triggering.

**Triggering** In order to identify an event in the detector, a certain threshold has to be set; and the read-out has to be activated only if this threshold is exceeded. Usually a fast signal is used for that, because it ensures correct timing. A discriminator is used to set a threshold and produce a logic signal, which has to be delayed by the right amount to trigger the peak of the slow signal. In the following sections specifying the setup at the individual beam-times, the further processing of this trigger signal is described.

**Dynamic Range** The dynamic range of the individual amplifiers is determined by the range, in which an incoming signal is amplified by a constant factor. For the whole setup this should hold for the deposited charge in the detector too. The dynamic range of the amplifiers is only one contribution here. The charge collection in the detector itself is also not complete and depending on the charge produced per volume. On the electronic side the linearity of the channel analyser and all the components processing this slow main signal have to be considered. The fast triggering channel can also affect the dynamic range, either by the disability to trigger on certain pulse-heights or due to timing shifts, which can lead to an amplitude loss, if the gate is not adjusted widely enough. The change due to the resistor-chain readout, used in both beam times for the thick detector, is discussed at the end of the following section.

## B.2 Resistor-Chain Readout

For the readout of a micro-strip detector, the usage of an individual readout chain for each strip, requires an advanced technology to produce vacuum compatible preamplifier boards with the dimensions of the detector pitch or vacuum-connectors with a huge amount of cables in the vacuum. Apart from the amount of work which would be needed, this and all the other components of the readout would also increase the prise of the setup by a large amount. The 80 strips and later 200 strips (see table A.2 on page 49) to be read out illustrate the effort, which would have been done, if we would not have used a resistor-chain readout for this purpose.

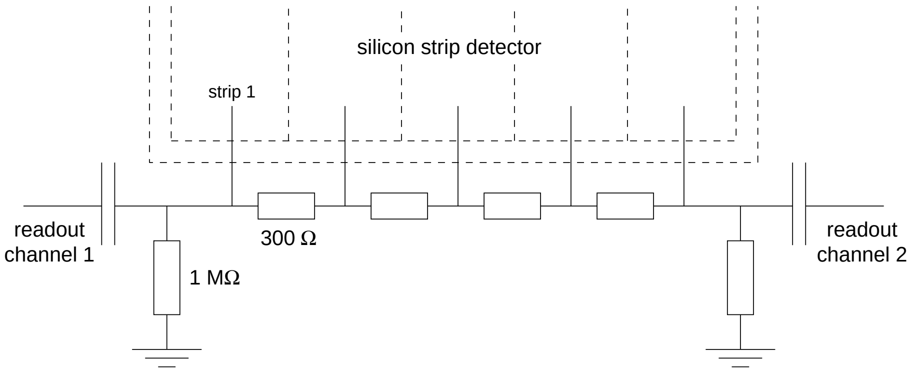


Figure B.1: Sketch of a resistor chain readout

In figure B.1 it is sketched, how each strip is connected to its neighbouring one by a defined ohmic resistor in this type of readout. Then two readout channels are sufficient to get energy and position of the incident particle. In chapter 2.4 on page 10 the position resolution obtained by this type of readout is discussed in detail. The dynamic range for deposited charges in the detector is unfortunately severely affected by this method. For a middle hit the charge is equally split into both pre-amplifiers, but for a hit in a strip at the edge of the detector the amplitude of the signal is divided by the amount of strips in the chain minus one in the most distant channel. As a signal in both channels is needed to determine total energy loss and position of the particle, the readout has to provide a dynamic range with a factor equally to the amount of the strips adding the range of deposited energies, that should be detected.

From the considerations in chapter 2.2 on page 8 on the energy range, which a thick last detector should cover, it is clear, that a huge dynamic range for the electronics is needed, if resistor chain readout is used. Hence we divided the readout chain at the ANKE beam time in four segments with 50 strips each, to cover an acceptable energy range.

## B.3 Test Beam Time in Cologne

We used a standard electronic setup, of which the general working scheme is sketched in figure B.2. The detector is connected via the pre-amplifier(PA) to the main amplifier, which incorporates a fast and a slow part. Shaping of the slow signal can be adjusted and the pulse is transferred to the peak sensing amplitude to digital converter(ADC), which converts it into a channel number. The fast bipolar output is discriminated in a constant fraction discriminator(CFD) and used as trigger opening a gate in which the ADC is read out. For simplicity other elements, like time delays to shift and adjust gating times, and a CAMAC-controller to provide gate and readout for the ADCs, are not shown in the figure below.

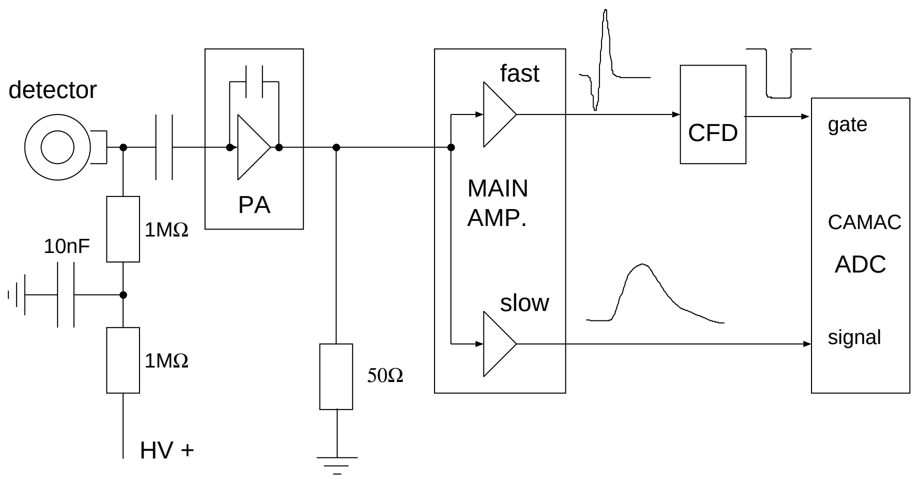


Figure B.2: Sketch of the electronic setup at Cologne

Four such channels were used at the beam time with the components listed in table B.1 on the following page.

## B.4 ANKE Beam Time

We used a completely different set of electronics at this beam time. The pre-amplifiers(PA) were directly mounted to the vacuum-flange to reduce cable length to a minimum for non-vacuum compatible electronics. But schematically they remained the same. Therefore they are not sketched in figure B.3. The fast and slow main amplifiers(MA) were situated in different modules and could be adjusted independently. The slow signal from the main amplifier was transferred to a stretcher module, which holds the maximum signal amplitude in the given gate by the discriminator(CFD). We can use some time delays(TD) to produce a gate with a fixed width for the digital converter(QDC). Within the gate width the QDC accumulates the charge obtained from the stretcher and converts the integrated charge into a channel number. The essential components are sketched in figure B.3.

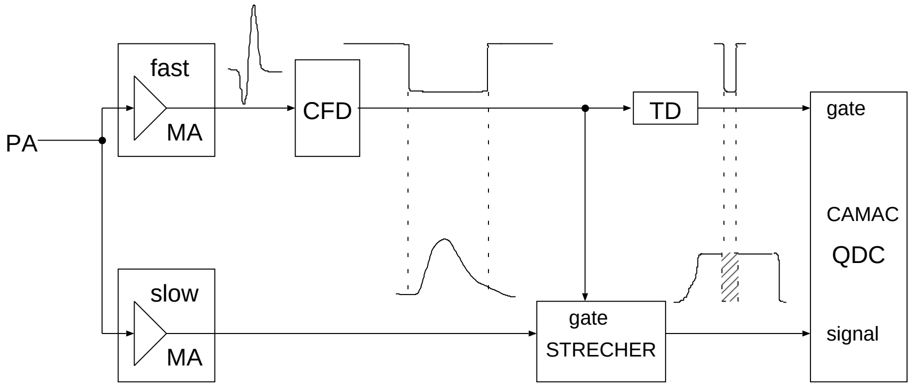


Figure B.3: Sketch of the electronic setup at ANKE

The forty-one channels used at the ANKE beam time in September '99 were set up in this fashion with most electronics being multi-channel devices, as listed in the table below.

| | Cologne | ANKE |
|---|---|---|
| pre-amplifier | Canberra 2003BT | ?? CSPA02 |
| main amplifiers | Tennelec TC 205A | 16 ch. fast shaper NEL 4.16.02.1 |
| | ORTEC 572 | 16 ch. shaper NEL 4.16.01.0 |
| discriminator | ORTEC timing SCA 420A | PS octal discr. 710 |
| time delay | C.A.E.N dual timer 2255 | |
| stretcher | none | LeCroy 3309 PTQ |
| channel analyser | Silena ADC 4418/V | LeCroy 4300B FERA |
| controller | CAMAC-FERA-PCI | |

Table B.1: Electronic components

# Appendix C

# Simulated $\omega$-Production Including Background

Using the geometry from the spectator setup and the forward detectors, a simulation was done for the proposed reaction: pd$\rightarrow$ d$\omega$p$_{sp}$ and the background reactions: pd$\rightarrow$ d$\rho$p$_{sp}$ and pd$\rightarrow$pXp$_{sp}$ [2].

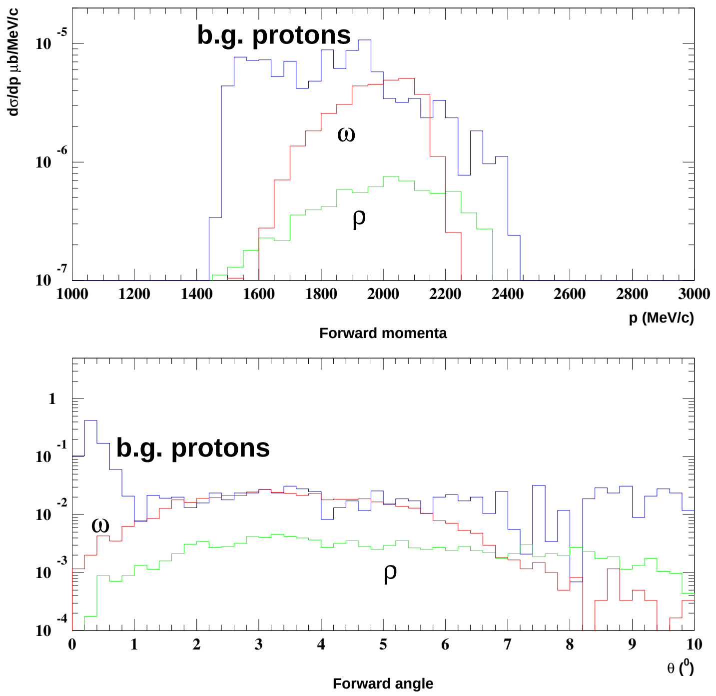


Figure C.1: Expected momentum and angular spectra of deuterons from $\omega$- and $\rho$-production and background protons in the forward counters [2]

The background from the production of the scalar $\eta$-meson can be suppressed by kinematical cuts. The $\rho$ meson is only slightly lighter than the $\omega$ meson and it has a width of 150 MeV, which is much wider than the width of the $\omega$ of 8.4 MeV. Therefore the reaction: pd$\rightarrow$d$\rho$p$_{\mathrm{sp}}$ will always contribute at least 20% to the $\omega$-channel [2].

At energies around 900 MeV the identification of deuterons against protons is a tricky task. To estimate the ratio of protons which can be misidentified, the background cross section for the misidentification of pd$\rightarrow$pXp$_{\mathrm{sp}}$ as pd$\rightarrow$d$\omega$p$_{\mathrm{sp}}$ was also simulated.

Not including any background from undesired reactions and scattering in the mechanical setup, the background is on the 1:1 level without particle identification in forward. Therefore a moderate proton suppression in forward should be sufficient for our purposes.

# Acknowledgements

I would like to thank:

- Prof. Dr. H. Ströher who has spent some weekends reading this theses as my referee and provided the possibility to do this work at the institute,
- Prof. Dr. W. Neuwirth for the consent to act as a co-referee,
- Dr. Ralf Schleichert for advice day and night, many fruitful discussions and contributions,
- Serguei Barsov for effective help in physical and practical problems, and valuable contributions to this work,
- D. Protić who produced and tested the thick micro-strip detectors and could help out answering questions,
- Andreas Mussgiller who developed the first version of the sorter for the data evaluation,
- A. Dewald, L. Steinert, Prof. Dr. H. Paetz gen. Schieck who provided many experimental tools and advises for the measurements at the Cologne-Tandem Accelerator,
- M. Büscher, Ye.S. Golubeva, L.A. Kondratyuk, A.K. Kacharava providing informations and contributions to this work and answering at lot of questions,
- P. Wieder, G. D'Orsaneo for excellent CAD drawings,
- The mechanical workshop at the IKP-Jüelich and at the IKP-Cologne for a lot of fast and nicely performed jobs,
- Michael, Maik, Serguei $\alpha$ to $\delta$, Vera, and many others at the institute who could help out with many odds and ends or just provided a good atmosphere,

and last but not least:

- Corinne and my friends and flatmates who endured this stressed guy for so long.

# Bibliography


[1] Bertolini, G., and Coche, A., Eds. *Semiconductor Detectors.* North-Holland Publishing Company - Amsterdam, 1968.

[2] Büscher M. et al. Study of $\omega$- and $\phi$-meson production in the reactions pd$\rightarrow$dVp$_{sp}$ at ANKE. COSY-Proposal #75, 1998.

[3] Collaboration CRN Strasbourg, IPN Orsay, LNS Saclay. Nouvelles de Saturne, 1995. F. Hibou et al.

[4] Ellis, J., Karliner, M., Kharzeev, D., and Sapozhnikov, M. Hadronic probes of the polarized intrinsic strangeness of the nucleon.

[5] Private comunication: Golubeva Ye.S.

[6] Hans, L. *Numerical data and functional relationships in science and technology.* Berlin : Springer, 1980.

[7] Iizuka, I. Prog. Theor. Phys. Suppl., 1966.

[8] Ipavich, F., Lundgren, R., Lambird, B., and Gloeckler, G. Measurement of Pulse-Height Defect in Au-Si Detectors ... *Nuclear Instruments and Methods*, 154 (1977), 291.

[9] Junghans, H., Koptev, V., and Büscher, M. Development of a K$^+$-Identification Procedure at ANKE. In *Annual Report.* Forschungszentrum Jülich, 1999.

[10] Private comunication: Kacharava A.

[11] Kacharava, A., Macharashvili, G., Nioradze, M., Komarov, V., Sopov, V., and Tchernyshev, V. Beam test of Cherenkov counter prototype for ZDF setup. *Nuclear Instruments and Methods A*, 10606 (1996), 356–360.

[12] Kacharava A. et al. Use of Cherenkov Counters in the ANKE Forward Detector. In *Annual Report.* Forschungszentrum Jülich, 1997.

[13] Knoll, G. F. *Radiation Detection and Measurement*, $2^{nd}$ ed. John Wiley & Sons, 1989.

[14] Lennard, W., Geissel, H., Winterbon, K., Phillips, D., Alexander, T., and Forster, J. Nonlinear Response of Si Detectors for Low-Z Ions. *Nuclear Instruments and Methods A*, 248 (1986), 454.

[15] LINDHARD, J., AND NIELSEN, V. Nuclear Collisions and Ionisation Fluctuations in Charged Particle Detectors. *Physics Letters* (1962).

[16] NYGA, K. Bestimmung der Spreading-Breiten der Isobar-Analog-Resonanzen... Master's thesis, Universität zu Köln, 1988. Anhang B.

[17] OBELIX COLLABORATION. Yad. Fiz., 1996.

[18] OKUBO, S. *Physics Letters B*, 5 (1963), 165.

[19] ORTEC. Silicon Detector Manual. referring to: C.F.WILLIAMSON, J.P.BOUJOT and J.PICARD, CEA-R-3042 (July 1966).

[20] PARTICLE DATA GROUP. *Review of Particle Properties*, particles and fields ed., vol. 45/II of *3*. The American Physical Society, June 1992. From: Physical Review D.

[21] WOLF, H. *Semiconductors*. Wiley, New York, 1971.

[22] ZIEGLER, J., BIERSACK, J., AND LITTMARK, U. *The Stopping and Range of Ions in Matter*, 96.xx ed. IBM-Research, April 1999.

[23] ZWEIG, G. CERN Report 8419/TH 412, 1964.